Redox Biology 68 (2023) 102960

Contents lists available at ScienceDirect

Redox Biology

journal homepage: www.elsevier.com/locate/redox

CXCR4-BTK axis mediate pyroptosis and lipid peroxidation in early brain injury after subarachnoid hemorrhage via NLRP3 inflammasome and NF-κB pathway

Chengli Liu [a,1], Kun Yao [a,1], Qi Tian [a,1], Yujia Guo [a], Guijun Wang [a], Peibang He [a], Jianfeng Wang [a], Jian Wang [b], Zhan Zhang [c,**], Mingchang Li [a,*]

[a] Department of Neurosurgery, Renmin Hospital of Wuhan University, Wuhan, 430060, Hubei, PR China
[b] Department of Anatomy, College of Basic Medical Sciences, Zhengzhou University, Henan, 450000, PR China
[c] Department of Rehabilitation Medicine, Renmin Hospital of Wuhan University, Wuhan, 430060, Hubei, PR China

ARTICLE INFO

Keywords:
Subarachnoid hemorrhage
Neuroinflammation
Pyroptosis
BTK
CXCR4
Lipid peroxidation

ABSTRACT

C-X-C chemokine receptor type 4 (CXCR4) is critical for homeostasis of the adaptive and innate immune system in some CNS diseases. Bruton's tyrosine kinase (BTK) is an essential kinase that regulates inflammation in immune cells through multiple signaling pathways. This study aims to explore the effect of CXCR4 and BTK on neuroinflammation in the pathogenesis of early brain injury (EBI) after subarachnoid hemorrhage (SAH). Our results showed that the expression of CXCR4 and p-BTK increased significantly at 24 h after SAH *in vivo* and in vitro. Ibrutinib improved neurological impairment, BBB disruption, cerebral edema, lipid peroxidation, neuroinflammation and neuronal death at 24 h after SAH. Inhibition of BTK phosphorylation promoted the in vitro transition of hemin-treated proinflammatory microglia to the anti-inflammatory state, inhibited the p-P65 expression and microglial pyroptosis. NLRP3 deficiency can significantly reduce pyroptosis in SAH mice. Moreover, CXCR4 inhibition can suppress NLRP3-mediated pyroptosis, NF-κB activation and NOX2 expression in vitro, and ibrutinib can abolish CXCR4-aggravated BBB damage and pyroptosis in EBI after SAH. The levels of CXCR4 in CSF of SAH patients is significantly increased, and it is positively correlated with GSDMD and IL-1β levels, and have a moderate diagnostic value for outcome at 6-month follow-up. Our findings revealed the effect of CXCR4 and P-BTK on NLRP3-mediated pyroptosis and lipid peroxidation after SAH *in vivo* and in vitro, and the potential diagnostic role of CXCR4 in CSF of SAH patients. Inhibition of CXCR4-BTK axis can significantly attenuate NLRP3-mediated pyroptosis and lipid peroxidation by regulating NF-κB activation in EBI after SAH.

1. Introduction

Aneurysmal subarachnoid hemorrhage (SAH) is a subtype of stroke with a high disability and mortality rates, and SAH caused by ruptured intracranial aneurysm accounts for 5–10% of strokes [1]. Early brain injury (EBI) within 3 days after SAH is the main cause of high mortality and poor prognosis [2]. SAH causes many physiological disorders during EBI, including decreased cerebral blood flow, increased intracranial pressure, and pathophysiological events, such as oxidative stress, neuroinflammation, and blood-brain barrier (BBB) dysfunction [3–5]. Numerous studies have demonstrated that innate inflammation, characterized by activation of resident microglia, infiltration of inflammatory cell, and release of cytokine, plays an important role in the pathogenesis of EBI following SAH [6]. Hence, neuroinflammation reduction is a promising approach to reduce EBI and promote neurological recovery after SAH.

Pyroptosis has been considered as an important and destructive pathophysiological process in EBI following SAH [7]. As an important member of the NLR family, NACHT Leucine-rich-repeat protein 3 (NLRP3) is mainly expressed in microglia [8]. The NLRP3 inflammasome consists of NLRP3, caspase-1, and the apoptosis-associated speck-like protein containing a CARD (ASC) [9]. After the assembly of

* Corresponding author. Department of Neurosurgery, Renmin Hospital of Wuhan University, Wuhan, 430060, Hubei, PR China.
** Corresponding author. Department of Rehabilitation Medicine, Renmin Hospital of Wuhan University, Wuhan, 430060, Hubei, PR China.
E-mail addresses: doctorzhang2003@163.com (Z. Zhang), Mingcli@whu.edu.cn (M. Li).
[1] These authors contribute equally to this study.

https://doi.org/10.1016/j.redox.2023.102960
Received 26 September 2023; Received in revised form 5 November 2023; Accepted 7 November 2023
Available online 10 November 2023

NLRP3 inflammasome activated by multiple stimulators, pro-caspase-1 is cleaved, and pro-IL-1β and pro-IL-18 are converted to mature forms that promote inflammatory response [9]. Moreover, activated caspase-1 efficiently cleaves gasdermin D (GSDMD) at an aspartate site within the linking loop, allowing the release of the N-terminal gasdermin (GSDMD-N), pausing its auto-inhibition and triggering pyroptosis. GSDMD-N oligomerizes and binds to phosphatidylserine in the inner leaflet of the cell membrane to induce membrane pore formation and secretion of IL-1β and IL-18 [10]. Numerous studies have shown that pyroptosis plays a vital role in inflammation following SAH [11,12]. Therefore, it is essential to understand the mechanism of pyroptosis to reduce SAH injury.

Bruton's tyrosine kinase (BTK) is a key regulator of B cell receptor functions and signaling transduction that regulates cell survival and proliferation [13]. Nevertheless, multiple studies have demonstrated the anti-inflammatory role of BTK, which is highly expressed in monocytes/macrophages [14]. BTK phosphorylation was believed to play an important role in toll-like receptors (TLR) signal transduction, leading to NF-κB activation [15–17], and is also involved in regulating the assembly of NLRP3 inflammasome in macrophages [14,18]. Recent studies demonstrated that activated NF-κB signaling pathway promote the transcription of inflammasome-related components, such as, GSDMD, NLRP3, pro-IL-18, and pro-IL-1β [19–21]. Hence, BTK phosphorylation plays important role in regulating NLRP3 inflammasome formation and pyroptosis in multiple ways. Ibrutinib is an irreversible inhibitor of BTK that inactivates the kinase domain of BTK, thereby dephosphorylating BTK, and inhibiting downstream signaling proteins [22]. Ibrutinib was used to suppress oxidative stress and inflammatory responses in microglia and neutrophils [13,23]. Accordingly, we hypothesized that BTK phosphorylation could mediate pyroptosis in SAH by regulating NLRP3 inflammation.

Chemokines are involved in the regulation of neuroinflammation. C-X-C chemokine receptor type 4 (CXCR4) is expressed in immune cells and hematopoietic cells, and is also present in the central nervous system, such as microglia, astrocytes and neurons, which mediates microglia activation and leukocyte migration to sites of brain injury [24]. Some studies have found that the inhibition of CXCR4 can alleviate microglia activation, neuroinflammation and pyroptosis, and improve neurological function after stroke in mice [25–27]. However, the mechanism of its action in improving neuroinflammation remains unclear. Previous studies have shown that phosphorylation of BTK can be directly regulated by CXCR4 in B-cell malignancies and arterial thrombosis [28,29]. Further exploration of the role of CXCR4 and BTK in microglial activation and pyroptosis after SAH is warranted.

Therefore, to investigate the effect of CXCR4 and BTK on neuroinflammation in pathogenesis of EBI after SAH, we explored the association between CXCR4-BTK and pyroptosis-related pathways. We hypothesized that BTK phosphorylation mediated by CXCR4 could regulate the activation of both NF-κB and the NLRP3 inflammasome after SAH, resulting in pyroptosis and neuroinflammation in EBI following SAH.

2. Material and methods

2.1. SAH patients and CSF sample

The study protocol (WDRY2021-K070) was approved by the Ethics Committee of Renmin Hospital of Wuhan University. As previously described [30], this research included forty SAH patients admitted to Renmin Hospital of Wuhan University within 3 days of their SAH onset from October 2021 to September 2022. Cerebrospinal fluid (CSF) sample from ten patients with normal-pressure hydrocephalus served as control. All patients received standard medical care after admission. The modified Rankin Scale (mRS: 0–6 score) was used to evaluate patient prognosis at the 6-month follow-up. Poor and good outcomes were defined as mRS scores $\geq$3 and < 3, respectively. The CSF samples were instantly centrifuged at 3000 rpm for 10 min at 4 °C, and after serum isolation, they were frozen at −80 °C for later use.

2.2. Cytokine measurements

Levels of CXCR4, GSDMD and IL-1β were measured in human CSF using ELISA kits (Bioswamp, China) according to the manufacturer's instructions.

2.3. Animals models of SAH

The Animal Center of Wuhan University provided 20–25g adult male C57BL6/J mice. NLRP3$^{-/-}$ mice were purchased from Model Animal Research Centre of Nanjing University (Guangzhou, China). They were housed in standard conditions of 22°C and 50–60% relative humidity with a 12h light/dark cycle and free access to food and water. Animal experiments were approved by the Institutional Animal Care and Use Committee of Wuhan University (WDRM-20221001A). SAH mice model was performed by endovascular perforation method [31]. Mice were anesthetized with 1% pentobarbital sodium (50 mg/kg). The artery in the left neck was exposed in the median neck incision. The left common carotid artery and the left external carotid artery were ligated, and a nylon monofilament was inserted 1 cm from the distal end of the common carotid artery, pushing the monofilament forward for about 2 mm upon feeling resistance, and withdrawn immediately after perforation. The sham group underwent the same surgical procedure without an endovascular puncture. Mice were intraperitoneally injected with ibrutinib (dissolved in 1% DMSO, MCE, USA) immediately after SAH. SAH group was given the same amount of 1% DMSO. For survival analysis experiments, ibrutinib was injected daily at the same dose. Mice were stereotaxic microinjected with lentiviral particles (GeneChem Co. Ltd., China) containing lentivirus overexpressing CXCR4 (OE-CXCR4) or its negative control oligonucleotide (OE-NC) at a dose of 2.0 μL (5×10^8 TU/mL) into the left cerebral cortex 7 days before SAH onset. The stereotaxic coordinates are as follows: point 1, anteroposterior 0.3 mm from the bregma, mediolateral 3 mm from the midline, and dorsoventral 2 mm from the skull; point 2, anteroposterior 0.8 mm from the bregma, mediolateral 3 mm from the midline, and dorsoventral 2 mm from the skull [32]. The injection speed was 0.2 μL/min, and the needle was left in place for 5 min after the injection. The grouping of animal experiments is shown in Supplement Fig. 1.

2.4. SAH grading

The SAH grading score was assigned 24 h after SAH [31]. Briefly, the basal cistern was divided into six segments, scored from 0 to 3 based on the volume of subarachnoid blood. The total score ranges from 0 to 18. Mice with SAH grading scores below 8, were excluded from the study.

2.5. Behavioral tests

Neurological function was detected using the Modified Garcia score [33] and the Beam Balance score [34] at 24 h after SAH. The Garcia score included six standards, each scoring 0–3. The total score ranges from 3 to 18. In the beam balance experiment, the ability of mice to walk on a narrow cylindrical wooden beam for 60 s was evaluated: 0 = no walking and falling; 1 = no walking, but staying on the beam; 2 = walking but falling; 3 = walking less than 20 cm; 4 = walking beyond 20 cm. The high neurological test scores indicated better neurological function.

2.6. Brain water content

Cerebral edema was evaluated by brain water content using the wet–dry method, as previously description [35]. Briefly, the brain was separated to the contralateral and ipsilateral hemispheres, and their wet

weight was determined. The cerebellum was used as an internal control. The samples were then dried at 100°C for 24 h and weighed to determine the dry weight. Brain water content was calculated as [(wet weight-dry weight)/wet weight] × 100 %.

2.7. Nissl's staining

Brain sections were stained with Nissl's staining to detect neuronal damage in CA1 as previously described [36].

2.8. Evans blue dying

The Evans blue extravasation method was performed to evaluate integrity of the BBB [37]. Evans blue dye (2% in saline) was injected into the tail at a rate of 5 ml/kg 2 h before sacrifice. The mice were perfused with normal saline, and the ipsilateral hemisphere was collected and homogenized in PBS, then centrifuged at 14000 rpm for 30 min in 4°C. The supernatant was collected, and incubated at room temperature for 1h with an equal amount of trichloroacetic acid. The sample was then centrifuged at 15000 rpm for 30 min at 4°C to separate the supernatant for quantification using a spectrophotometer at 610 nm. The results are shown as micrograms per milligram of brain weight.

2.9. Immunohistochemistry staining

Immunohistochemistry was performed using DAB substrate kit (Servicebio, China) [38]. First, brain sections were deparaffinized and then rehydrated with gradient ethanol to remove xylene:100% ethanol for 5 min, 95% ethanol for 5 min, 75% ethanol for 5 min, and washed three times with deionized water for 5 min. To block peroxidase, sections were incubated in 3% H_2O_2 for 20 min, washed three times with PBS for 5 min, and then immersed with 0.5% Triton-X 100 for 30 min and blocked with 5% BSA for 60 min at room temperature. The slices were incubated with the primary antibodies of Rabbit anti-NLRP3 (1:200, Abcam, Ab270449) at 4 °C overnight. Sections were washed three times with PBS and incubated with secondary antibodies for 1 h at room temperature. Acceptable staining intensity was obtained using a DAB kit. The slides were treated with DAB reagent for 1–5 min, washed with PBS for 15 min, counterstained with hematoxylin for 2 min, rinsed with tap water for 15 min, then dehydrated with gradient ethanol and xylene, and mounted for observation.

2.10. Primary microglial culture

Primary microglia were isolated and purified from C57BL6/J mice within 3 days of birth as described previously [39]. Briefy, cerebral cortex was isolated, fltered through a 70-μm nylon mesh, and then cultured in low-glucose DMEM medium supplemented with 10% FBS and 1% penicillin/streptomycin at 37°C under 5% CO2 incubator. On day 12, cells were treated with mild trypsin digestion (1 M $CaCl_2$, 0.5 M EDTA, and 0.25% trypsin-EDTA in low-glucose DMEM medium) for 45 min in the incubator. After washing with PBS for 3 times, primary microglia were extracted by 0.25% trypsin–EDTA and centrifuged at 2000 rpm for 10 min before cultivation. The purity of primary microglia was calculated using the following formula: [primary microglial purity (%) = (CD11b- and DAPI-positive cells/DAPI-positive cells) × 100%].

2.11. Cell culture and SAH model in vitro

BV2 cells and primary microglia were cultured in a complete medium containing DMEM with high glucose, 10% FBS and 1% penicillin/streptomycin at 37°C under 5% CO2. Cells treated with a complete medium containing 120 μM Hemin (MCE, China) and vehicle for 24h was used to mimic the SAH model in vitro. Cells were treated with different concentrations of Ibrutinib and AMD3100. The optimal concentration of Ibrutinib and AMD3100 for subsequent administration to BV2 cells was 10uM.

2.12. Cell viability and dead/live assay

Cell viability was measured using the CCK-8 kits according to the manufacturer's instructions (MCE, USA). In the dead/live experiment, BV2 cells were washed with PBS and then incubated with PBS with PI (4 μM) and calcein-AM (3 μM) for 30 min darkness. Cells were washed again and observed under a fluorescence microscope.

2.13. Determination of the levels of oxidative stress

To detect the reactive oxygen species (ROS) level in cells, 2′,7′-dichlorofluorescin diacetate (DCFH-DA; 10 μM, MCE, USA) was added to the complete medium and incubated in the dark for 30 min before observation under fluorescence microscope. The concentration of total SOD in brain tissues or BV2 cells was detected by an SOD assay kit (Nanjing Jiancheng Bioengineering Institute, China). The levels of MDA and GSH-Px in brain tissues was measured by the MDA and GSH-Px assay kits (Nanjing Jiancheng Bioengineering Institute, China) according to the kit instructions [40].

2.14. Immunofluorescence staining

Mouse brains were fixed in 10% paraformaldehyde for 24 h and cut into 10 μm coronal sections. Cell slides were fixed with 4% paraformaldehyde for 10 min. The slices were incubated with 0.5 % Triton-X 100 for 30 min and then sealed with 5% bovine serum albumin for 1 h. Then, the slices were incubated with the primary antibodies of mouse anti-Iba (1:200, Proteintech, 66827-1-Ig), rabbit anti-CXCR4 (1:200, Beyotime, AF6621), rabbit anti-p-BTK (1:200, Affinit, AF0841), rabbit anti-GSDMD-N (1:200, Invitrogen, PA5-116745), rabbit anti-iNOS (1:200, Abcam, 13120S) and mouse anti-Arg1(1:200, Proteintech, 66129-1-Ig) at 4 °C overnight. After washing with PBS for 3 times, the sample was immersed with the appropriate secondary antibody (1:500, Jackson Immunoresearch) for 1.5 h. The tissue slices and cell slides were washed twice in PBS and then incubated in DAPI for 30 min. The sample were sealed with neutral resin after washing with PBS.

2.15. TUNEL staining

To detect neuronal death, double immunostaining of NeuN (1:200, Proteintech, 66836-1-Ig) and TUNEL was conducted by TUNEL Assay Kit (Beyotime, China) in coronal sections at 24 h after SAH according to the manufacturer's instructions.

2.16. Co-immunoprecipitation (CO-IP)

As described previously [41], the BV2 cells were lysed in IP buffer containing cocktail (MCE) for 30min and extraction followed by centrifugation for 15 min at 12000 rpm. A/G magnetic beads were pre-incubated with specific antibodies for 6h and washed three times. The cell lysate was then added and co-incubated for 2h. Subsequently, beads were washed three times. Immunoprecipitates were eluted by boiling with 1% SDS sample buffer for 10 min, and the supernatant was collected after centrifugation at 12000 rpm for 2 min. Subsequently, western blotting was used to determine whether binding the two proteins was possible.

2.17. Western blotting

The protein from ipsilateral cortical tissue and BV2 cells in each group were extracted and measured by a BCA protein assay. Equal amounts of protein were separated by electrophoresis on 8–12% SDS-PAGE gels. Proteins were transferred to PVDF membranes by electrophoresis. The membranes were sealed with 5% skimmed milk for 1 h.

Then, membranes were incubated overnight at 4°C with appropriate elementary antibodies, including rabbit anti-CXCR4 (AF6621, Beyotime), rabbit anti-BTK (21581-1-AP, Proteintech), rabbit anti-p-BTK (AF0841, Affinit), rabbit anti-Occludin (ab31721, Abcam), rat anti-ZO-1 (Sc-57535, Santa Cruz Biotechnology), rabbit anti-ASC (10500-1-AP, Proteintech), rabbit anti-NLRP3 (Ab270449, Abcam), rabbit anti-Caspase-1 (A16792, Abclonal), rabbit anti-GSDMD (PA5-116745, Invitrogen), rabbit anti–NF–κB p65/RelA (A2547, Abclonal), rabbit anti-

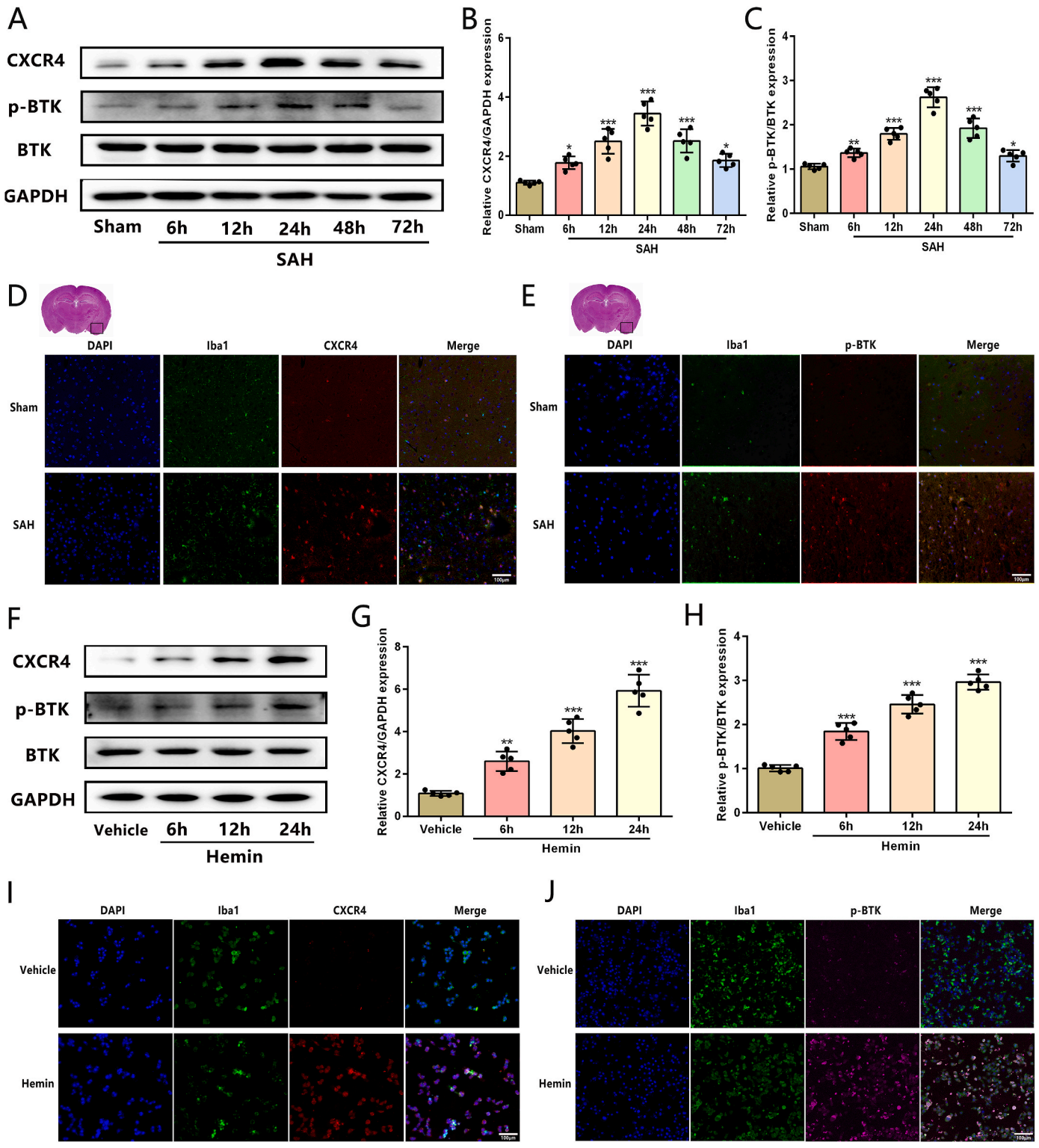

Fig. 1. The levels of CXCR4 and p-BTK in SAH mice model and in vitro hemin-treated BV2 cells (A–C) Western blot showing CXCR4, p-BTK and BTK expression at 6 h, 12 h, 24 h, 48 h, and 72 h following SAH onset (n = 5/group). (D–E) Co-staining of Iba (green) and CXCR4 (red) or p-BTK (red) was showed in microglia at 24 h after SAH (n = 3/group, original magnification × 200). (F–H) Western blotting images exhibiting expression level of CXCR4, p-BTK and BTK in hemin-treated BV2 cells in vitro (n = 5/group). (I–J) The level of CXCR4 and p-BTK detected by immunofluorescence staining in BV2 cells treated with hemin (n = 3/group, original magnification × 200). Data was represented as mean ± SD. $^{*}P < 0.05$, $^{**}P < 0.01$, $^{***}P < 0.001$ vs sham group.

p–NF–κB p65/RelA-S536 (AP0124, Abclonal) , rabbit anti-IL-1β (A16288, Abclonal), rabbit anti-IL-18 (Ab191152, Abcam), rabbit anti-TNF-α (17590-1-AP, Proteintech), rabbit anti-iNOS (13120S, Abcam), mouse anti-Arg1 (66129-1-Ig, Proteintech), rabbit anti-CD206 (A8301, Abclonal), rabbit anti-NOX2 (A22149, Abclonal) and mouse anti-GAPDH (MAB45855, Bioswamp). After washing with TBST, membranes were incubated with horseradish peroxidase (HRP) -conjugated secondary antibodies (Goat anti-Mouse IgG, Goat anti-Rabbit IgG and Goat anti-Rat IgG) at room temperature for 1 h. Immunoreactivity was evaluated using an enhanced ECL kit (Biosharp). Immunolabeling was scanned with the chemiluminescence imaging system and data were normalized by GAPDH or albumin.

2.18. Statistical analysis

All results were analyzed by the GraphPad Prism software (version 5.04) and were showed as the mean ± standard deviation (SD). Differences between the two groups were evaluated by student's t-tests. Multiple groups differences were assessed by one-way ANOVA analysis followed by Tukey's post hoc test. Pearson's correlation test was applicated to assess the correlation between CXCR4 and GSDMD, IL-1β, and mRS scores. The area under the ROC curve and the sensitivity and specificity of CXCR4 were evaluated. $P < 0.05$ was considered a statistically significant difference.

3. Results

3.1. The increased expression level of CXCR4 and p-BTK in the ipsilateral cortex in SAH mice and hemin-treated microglia

To confirm the role of CXCR4 and p-BTK after SAH, we measured the protein levels of CXCR4, p-BTK and BTK in the ipsilateral cortex among groups after SAH. Western blotting showed that the levels of CXCR4 and p-BTK significantly increased at 24 h, but the expression of total BTK is not obvious difference (Fig. 1A–C). Double immunofluorescence labeling of Iba with CXCR4 or p-BTK showed that the expression of CXCR4 or p-BTK in microglia was increased in SAH mice compared to sham mice (Fig. 1D and E). Similarly, western blotting showed that the expression level of CXCR4 and p-BTK was significantly enhanced at 24 h in BV2 cells treated with hemin (Fig. 1F–H). Immunofluorescence also showed that the level of CXCR4 and p-BTK was significantly upregulated in hemin-treated BV2 cells (Fig. 1I and J). These results indicated that CXCR4 and p-BTK may be involved in microglia activation after SAH. To further verify the role of microglia in SAH, we extracted and purified primary microglia from young C57BL6/J mice. CD11b was used to identify the purity of microglia, and the purity of cells was greater than 95% (Supplemental Fig. 3A). Western blot and immunofluorescence were also used to detect the expression of CXCR4 and p-BTK (Supplemental Figs. 3B–E). The expression of CXCR4 and p-BTK was significantly increased in primary microglia after hemin treatment, and the trend was similar to that of BV2 cells.

3.2. BTK phosphorylation inhibition attenuated neurological impairment, lipid peroxidation and neuroinflammation in SAH mice

Ibrutinib, a specific inhibitor of BTK phosphorylation, was administrated to evaluate the role of p-BTK in EBI following SAH. The SAH grading score between the SAH and SAH + ibrutinib groups showed no statistical difference (Fig. 2A and B). Of the total 381 mice used, 268 mice underwent SAH induction of which 71 (26.49%) rats died after SAH (Supplemental Fig. 2A). The neurological scores of modified Garcia and beam balance were significantly reduced at 24 h after SAH in the SAH + vehicle and SAH + Ibru (1 mg/kg) groups. However, administration of ibrutinib (20 mg/kg) significantly improved the neurological deficits (Fig. 2C and D). Based on these results, the optimal dose of ibrutinib was 20 mg/kg, which was used for the rest of the experiments. These results showed significant neurological impairments in SAH mice, while ibrutinib (20 mg/kg) treatment significantly improved neurological performance at 24 h after SAH. Both the sham and ibrutinib groups had 100% survival within seven days. However, post-SAH mice showed 30% survival (4 of 10 mice survived) by day 7. The survival curve displayed a significant improved survival rate in the SAH + ibrutinib (20 mg/kg) groups (8 of 10 mice survived) (Fig. 2E). The water content of the left and right hemispheres of the brain increased significantly after SAH, and ibrutinib could significantly reduce cerebral edema (Fig. 2F). Moreover, SAH injury significantly increased MDA levels and decreased the activity of SOD and GSH-Px, and ibrutinib could reduce MDA levels and increase the activity of SOD and GSH-Px in SAH mice (Fig. 2G–I). Western blot results showed that the expression of NOX2, p-P65, IL-1β, IL-18 and TNF-α was significantly increased in the SAH group, whereas ibrutinib administration inhibited NOX2, p-P65, IL-1β, IL-18, and TNF-α expression (Fig. 2J-O).

3.3. BTK phosphorylation inhibition reduced BBB permeability and neuron injury in SAH mice

BBB permeability was measured by Evans blue dying and the levels of tight junction proteins, including occludin and ZO-1. Decreased expression of occludin and ZO-1 was found in the ipsilateral cortex of SAH mice, and ibrutinib significantly reduced the disruption of occludin and ZO-1 (Fig. 3A–C). Furthermore, EB extravasation was remarkable increased in the SAH + vehicle group, whereas ibrutinib significantly decreased EB dye leakage in both hemispheres compared to the SAH + vehicle group at 24 h after SAH (Fig. 3D). Representative images showed the extravasation of the EB dye at 24 h after SAH (Supplemental Fig. 2B). The cerebral structure of the hippocampus in SAH group revealed obvious tissue damage and a significantly reduction in the number of Nissl positive cells, treatment with ibrutinib ameliorated histological injury and neuron damage compared to the SAH group at 24 h after SAH (Fig. 3E and F). In addition, to clarify the neuroprotection of ibrutinib, TUNEL staining showed significant neuronal death in the cortex after SAH, and ibrutinib treatment can reduce the number of neuron death at 24 h after SAH (Fig. 3G and H).

3.4. BTK phosphorylation inhibition suppressed inflammation in hemin-treated BV2 cells in vitro

BV2 cells were treated with different concentrations of ibrutinib to confirm the effect of BTK on them. CCK-8 kits were used to detect cell viability of BV2 cells treated with ibrutinib for 24 h (Fig. 4A). The results found that ibrutinib significantly increased BV2 cell viability in a concentration dependent manner with an optimum treatment concentration of 10uM. Dead/live assay also implicated that ibrutinib can relieve hemin-induced BV2 injury in vitro (Fig. 4B). Western blotting was used to evaluated the inflammation level of BV2 cells. The data revealed that hemin treatment significantly upregulated the expression of NOX2, p-P65, IL-1β, IL-18, and TNF-α in BV2 cells, and this increase was significantly inhibited by ibrutinib treatment (Fig. 4C–H). CD206, iNOS and Arg1 expression was analyzed by western blotting and immunofluorescence to investigate further the effect of ibrutinib on BV2 cell subtypes (Fig. 4I-M). The results demonstrated that hemin-treated BV2 cells trend to polarize towards the M1 phenotype with the upregulation of p-P65, IL-1β, TNF-α and iNOS, whereas ibrutinib can promote M2 polarization with the upregulation of Arg1 and CD206 and the downregulation of p-P65, IL-1β, TNF-α and iNOS. To further explore the effect of Ibrutinib on microglial polarization, we again performed experiments using primary microglial cells. The results of western blotting showed that the expressions of p-P65, iNOS, TNF and IL-1β were significantly increased after hemin treatment of primary microglia, showing M1 polarization. After treatment with Ibrutinib, the expression of p-P65, iNOS, TNF and IL-1β was significantly decreased, while Arg1 and CD206 expression was significantly increased, which was manifested as M2 polarization

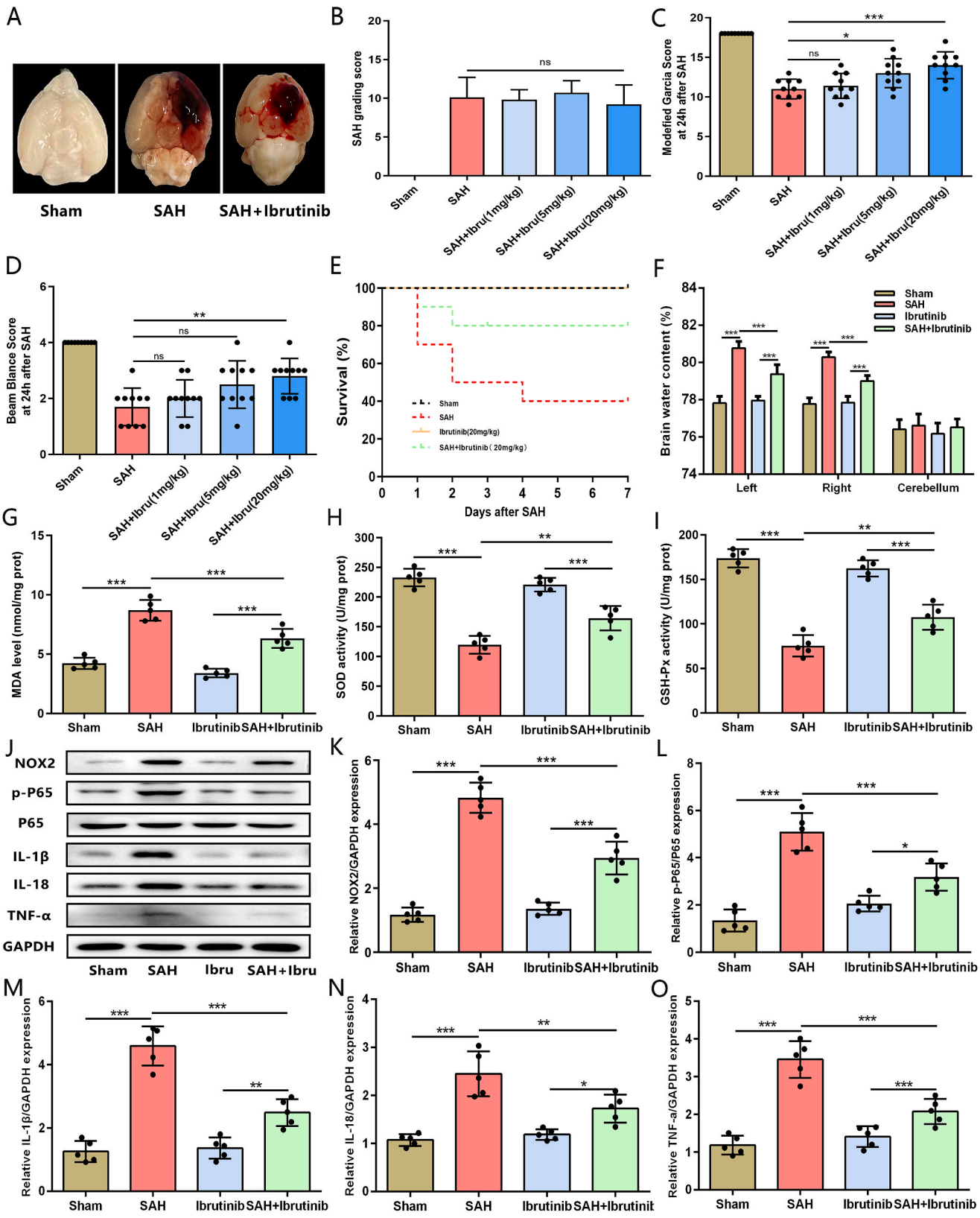

Fig. 2. Ibrutinib reduced neurological impairment , lipid peroxidation and inflammation at 24 h after SAH in mice (A) Schematic diagram of SAH. (B) SAH grading score of each group (n = 10/group). (C–D) Bars show changes in modified Garcia score and balance beam score in SAH mice after administration of different drug concentrations (n = 10/group). (E) Survival curve of each group (n = 10/group). (F) Bar graphs showed cerebral edema in the left hemisphere, right hemisphere and cerebellum at 24 h after SAH (n = 5/group). (G–I) Bar graphs showed the levels of MDA, SOD and GSH-Px in the ipsilateral cortex at 24 h after SAH (n = 5/group). (J–O) Western blotting images and quantitative data of relative expression level of NOX2, p-P65, P65, IL-1β, IL-18 and TNF-α in the ipsilateral cortex after SAH (n = 5/group). Data was represented as mean ± SD. * mean $P < 0.05$, ** mean $P < 0.01$, *** mean $P < 0.001$ vs sham group.

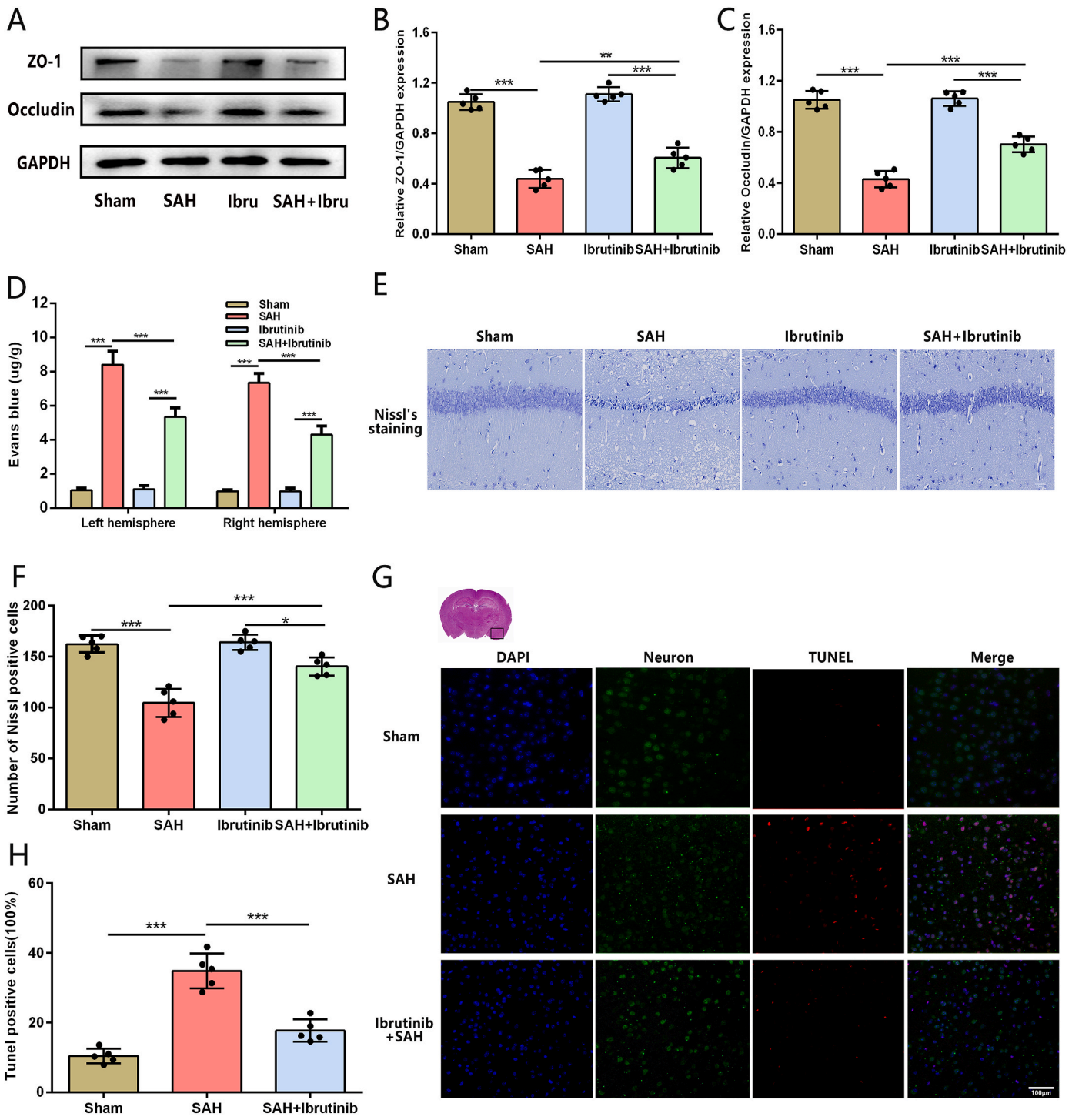

Fig. 3. Ibrutinib reduced BBB damage and neuron injury at 24 h after SAH in mice (A–C) Western blotting images and quantitative data of relative expression level of ZO-1 and occludin in the ipsilateral cortex after SAH (n = 5/group). (D) Bar graphs showed the content of the Evans blue in the left and right hemispheres (n = 5/group). (E–F) Histopathological changes detected by Nissl's staining in CA1 of the hippocampus (original magnification × 200) (n = 5/group). (G–H) TUNEL staining and bar graph showed the level of neuron death tested by TUNEL assay in the ipsilateral cortex at 24 h after SAH (n = 5/group, original magnification × 200). Data was represented as mean ± SD. * mean $P < 0.05$, ** mean $P < 0.01$, *** mean $P < 0.001$ vs sham group.

(Supplemental Figs. 4A–G). Immunofluorescence of Arg1-iNOS in primary microglia further verified our conclusion (Supplemental Fig. 4H). These results further showed the tendency of M1 polarization after hemin treatment and Ibrutinib promoted the tendency of M1 to M2 polarization of primary microglial cells after hemin treatment.

3.5. BTK phosphorylation inhibition ameliorated pyroptosis and lipid peroxidation in hemin-treated BV2 cells in vitro

To further confirm the mechanism of neuroinflammatory inhibition, COIP was applied to identify the interaction of p-BTK and NLRP3, and the results found that p-BTK is directly related to NLRP3, which indicated p-BTK can regulate NLRP3 inflammasome activation (Fig. 5A and

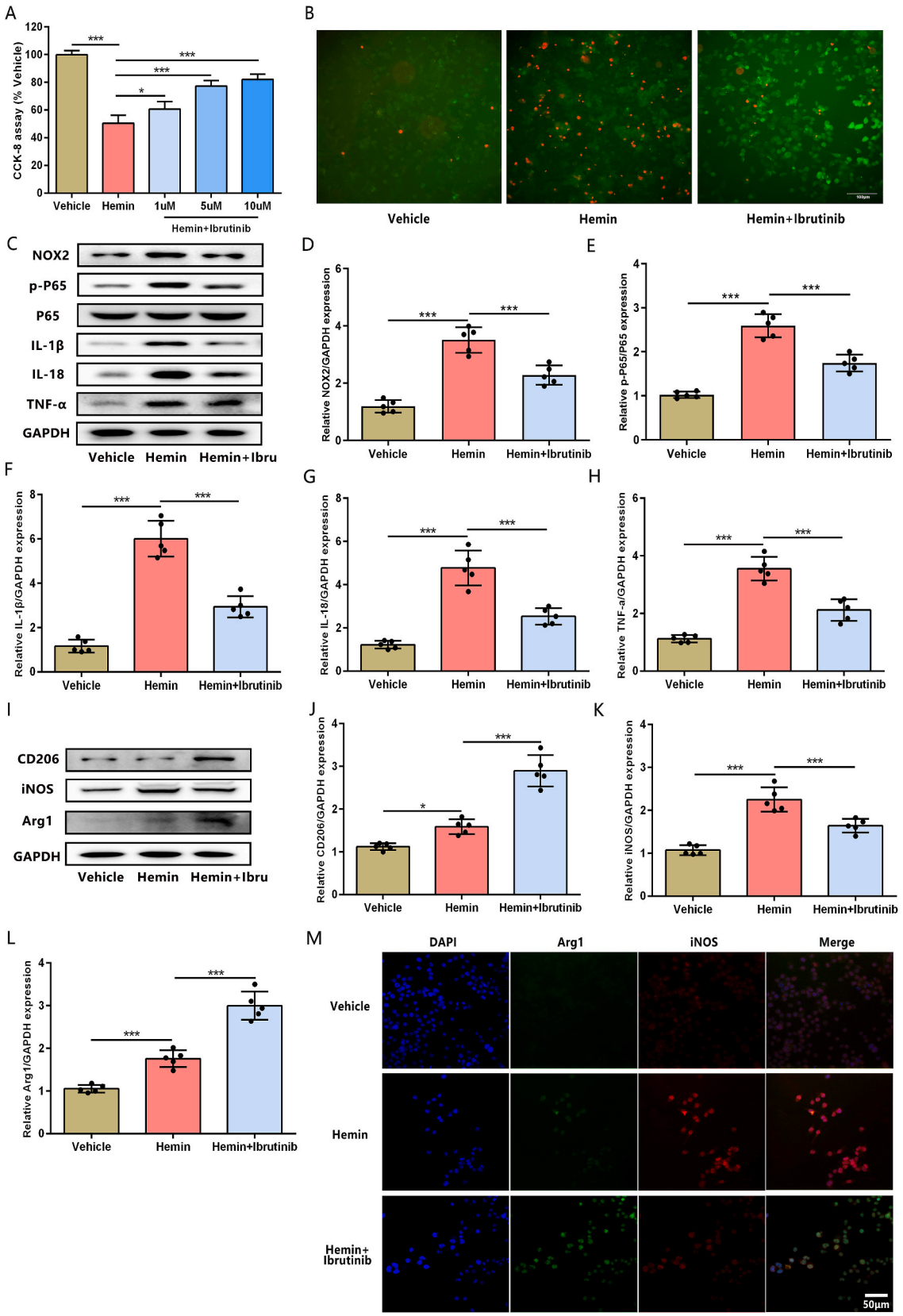

Fig. 4. Ibrutinib reduced inflammation and microglial polarization in BV2 cells (A) The viability of BV2 treated with different concentration of ibrutinib for 24 h was tested by CCK-8 assay in vitro (n = 6/group). (B) BV2 cells treated with hemin for 24 h were measured by Dead (red)/Live (green) assay in the presence and absence of ibrutinib (original magnification × 200). (C–H) Western blotting images and quantitative data of relative expression level of NOX2, p-P65, P65, IL-1β, IL-18 and TNF-α in hemin-treated BV2 cells (n = 5/group). (I–L) Western blotting images and quantitative data of relative expression level of CD206, Arg1 and iNOS in BV2 treated with hemin (n = 5/group). (M) The levels of iNOS and Arg1 detected by immunofluorescence staining in hemin-treated BV2 cells (original magnification × 400). Data was represented as mean ± SD. * mean $P < 0.05$, ** mean $P < 0.01$, *** mean $P < 0.001$ vs vehicle group.

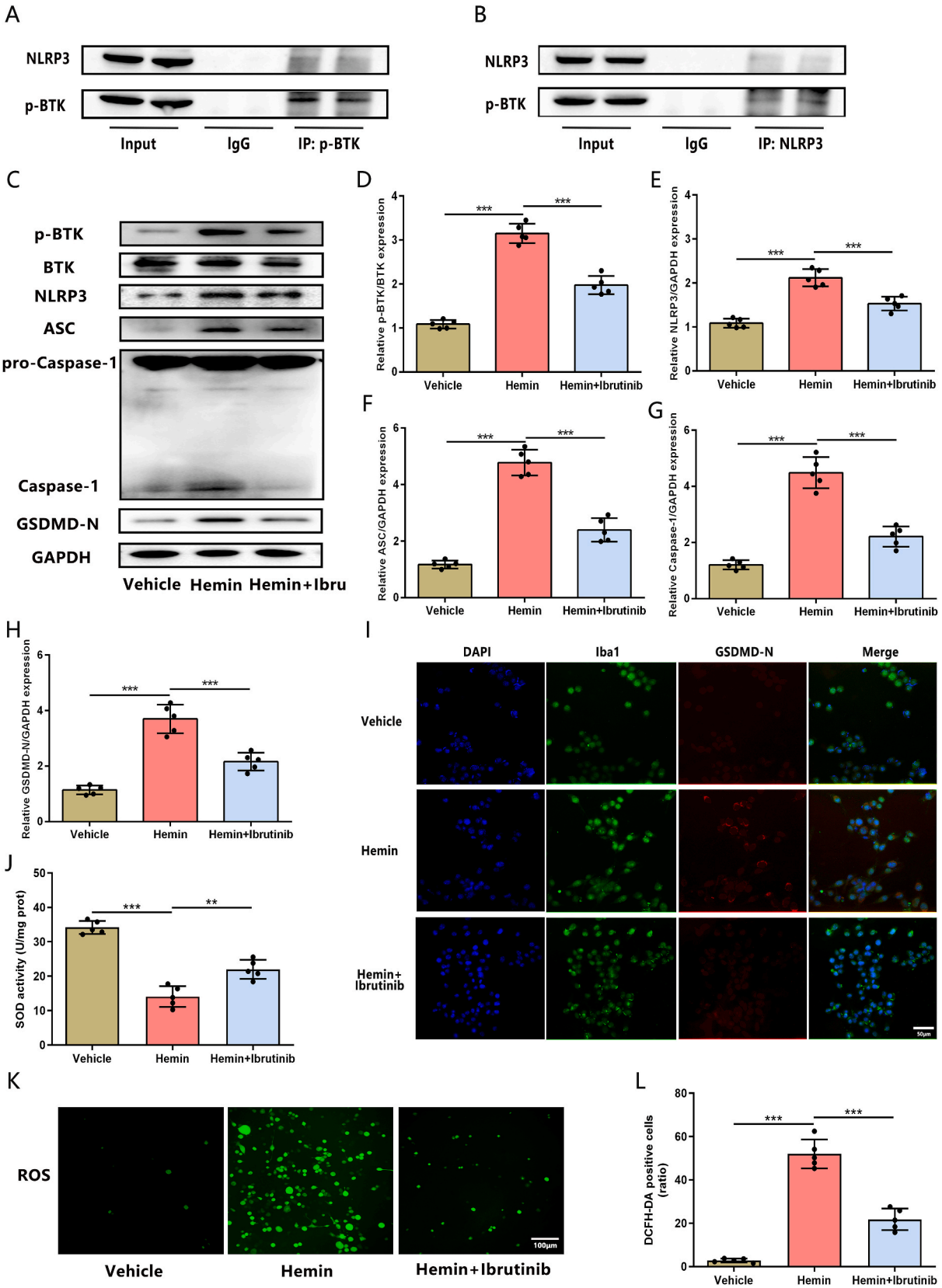

Fig. 5. Ibrutinib attenuated NLRP3-mediated pyroptosis and lipid peroxidation in hemin-treated BV2 cells in vitro (A–B) The interaction of p-BTK and NLRP3 tested by COIP in hemin-treated BV2 cells. (C–H) Western blotting images and quantitative data of relative expression level of p-BTK, BTK, NLRP3, ASC, caspase-1, and GSDMD-N in BV2 treated with hemin (n = 5/group). (I) The level of GSDMD-N detected by immunofluorescence staining in BV2 cells treated with hemin (original magnification × 400). (J) The activity of SOD in BV2 cells treated with hemin (n = 5/group). (K) Representative images of ROS expression detected by immunofluorescence in BV2 cells treated with hemin (original magnification × 200). (L) Quantitative analyses of the number of DCFH-DA-positive cells (n = 5/group). Data was represented as mean ± SD. * mean $P < 0.05$, ** mean $P < 0.01$, *** mean $P < 0.001$ vs vehicle group.

B). To confirm role of BTK phosphorylation in pyroptosis, western blotting was used to detect pyroptosis-related proteins. The results revealed that ibrutinib could significantly reduce the expression level of p-BTK, NLRP3, ASC, caspase-1 and GSDMD-N in hemin-treated BV2 cells in vitro (Fig. 5C–H). Double immunofluorescence labeling of GSDMD-N and Iba demonstrated that the level of GSDMD-N was upregulated in hemin-treated BV2 cells in vitro compared to that in vehicle group, and ibrutinib significantly reduced the expression of GSDMD-N (Fig. 5I). Moreover, the results found that ibrutinib can significantly increase the activity of SOD and reduce ROS levels in hemin-treated BV2 cells in vitro (Fig. 5J-L).

3.6. BTK phosphorylation inhibition reduced pyroptosis in SAH mice

Western blotting also showed that SAH significantly upregulated the expression level of p-BTK, NLRP3, ASC, caspase-1 and GSDMD-N compared to sham mice, and these effects were suppressed by ibrutinib treatment (Fig. 6A–F). Immumohistochemistry was used to detected the expression of NLRP3 in the ipsilateral cortex (Fig. 6G). The expression of NLRP3 significantly increased in neuron and microglial cells in SAH group compared to the sham group. However, ibrutinib ameliorated the upregulation of NLRP3 compared to the SAH group. These results indicated that inhibiting BTK phosphorylation can reduce pyroptosis by suppressing NLRP3 inflammasome formation in mouse.

3.7. NLRP3 deficiency reduced neuroinflammation and pyroptosis in SAH mice

NLRP3 knockout mice were used to investigate the role of NLRP3 in pyroptosis after SAH. Our results showed that higher Modified Garcia and lower brain water content in the left and right hemispheres were observed in NLRP3−/− SAH mice than in SAH mice at 24 h after SAH (Fig. 7A and B). Furthermore, NLRP3$^{-/-}$ SAH mice displayed the lower EB extravasation in the ipsilateral hemisphere compared with the SAH group (Fig. 7C). Representative images showed the extravasation of the EB dye at 24 h after SAH (Supplemental Fig. 2C). The expression of ZO-1 and occludin was higher in the ipsilateral cortex of NLRP3$^{-/-}$ SAH mice than in SAH mice 24 h after SAH (Fig. 7D–F), which implicated that NLRP3 knockout can protect the integrity of the BBB. NLRP3 knockout significantly inhibited the increase of caspase-1, GSDMD-N, IL-1β and IL-18 in ipsilateral cortex after SAH (Fig. 7D, G-K). These results indicated that NLRP3 inflammasome plays a vital role in pyroptosis after SAH.

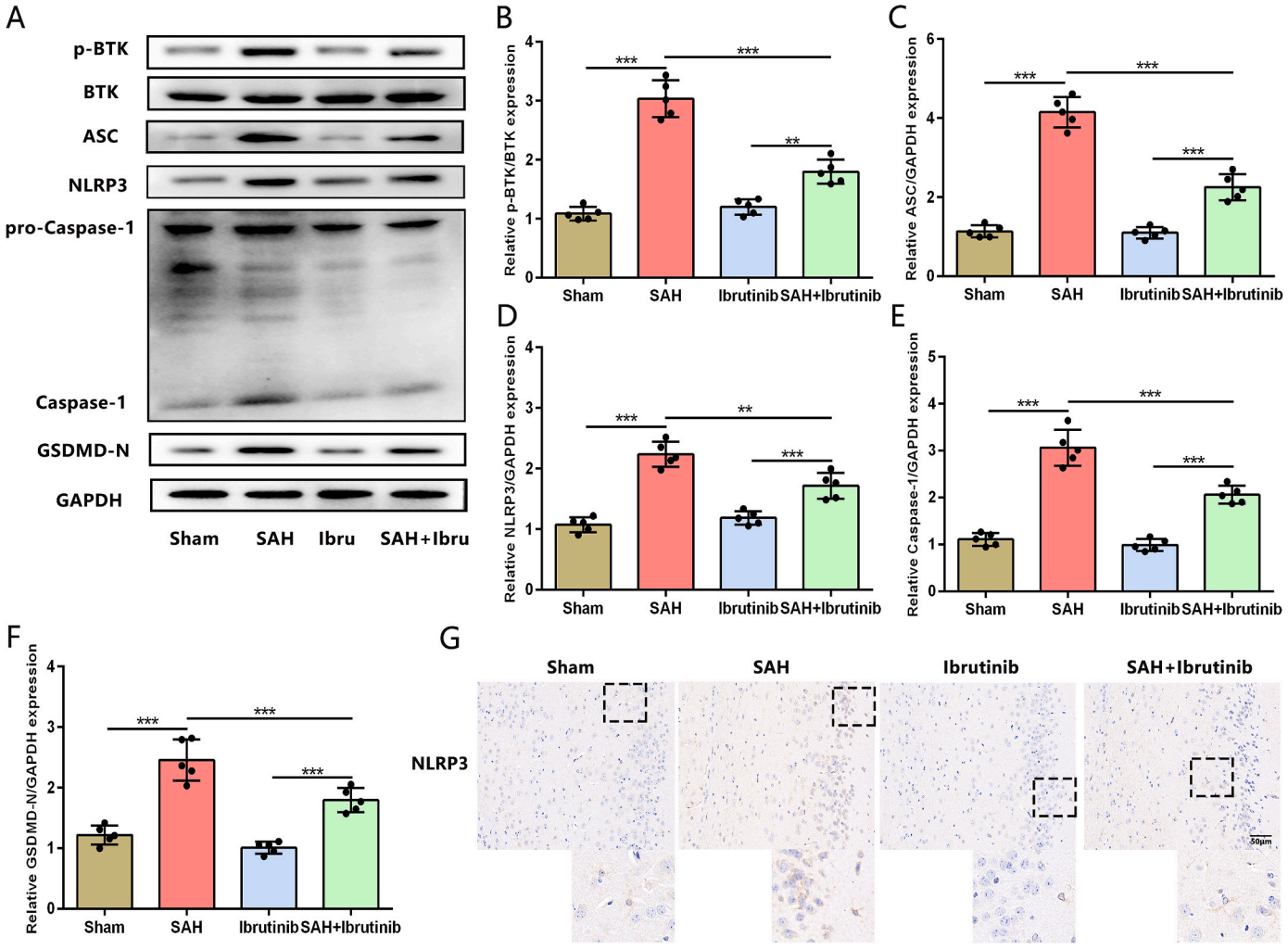

Fig. 6. Ibrutinib ameliorated pyroptosis in the ipsilateral cortex after SAH by inhibiting the formation of NLRP3 inflammasome (A–F) Western blotting images and quantitative data of relative expression level of p-BTK, BTK, NLRP3, ASC, caspase-1, and GSDMD-N in SAH mice (n = 5/group). (G) Representative images of NLRP3 expression detected by immunohistochemical staining in the ipsilateral cortex (original magnification × 400). Data was represented as mean ± SD. * mean $P < 0.05$, ** mean $P < 0.01$, *** mean $P < 0.001$ vs sham group.

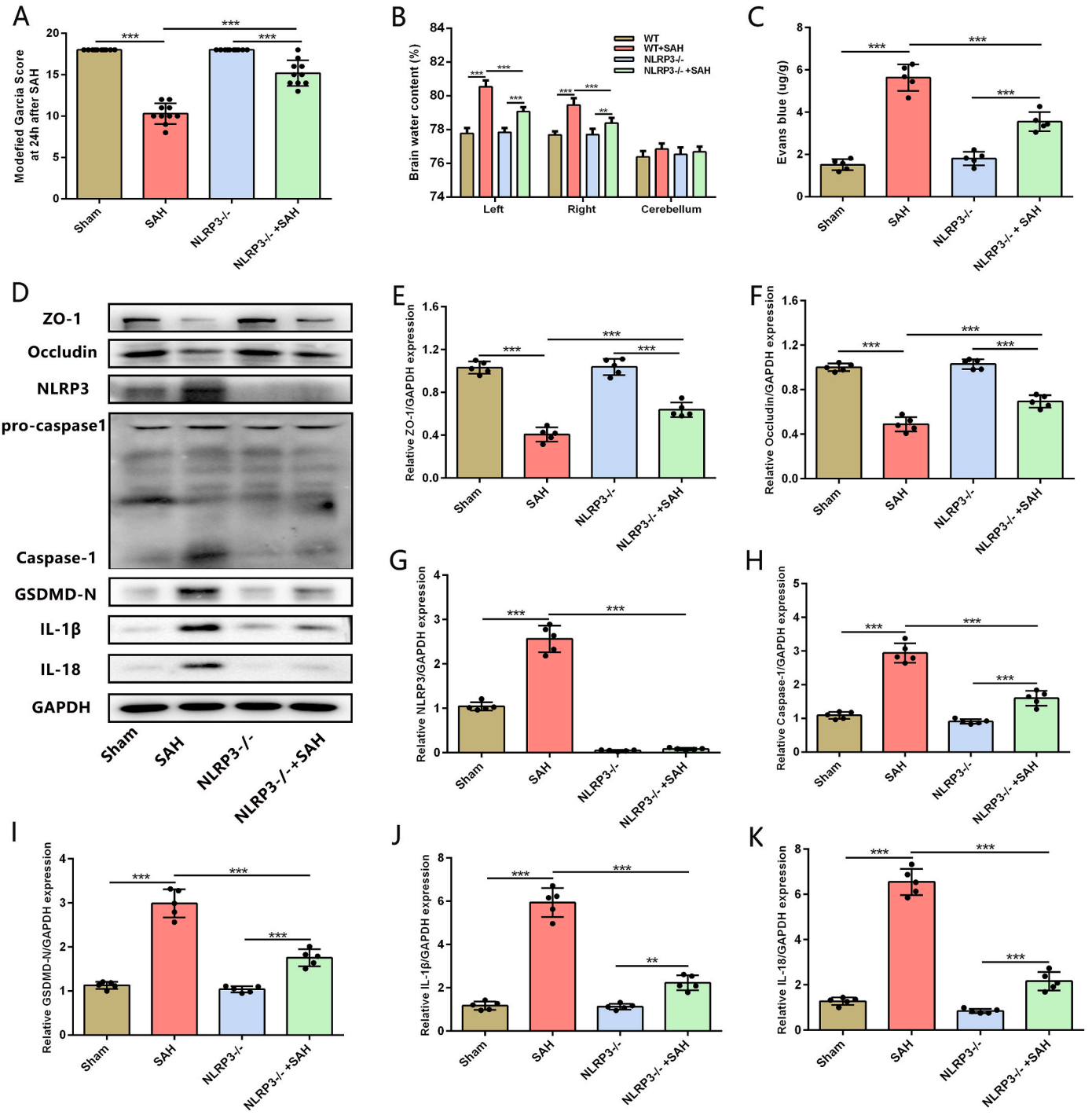

Fig. 7. NLRP3 deficiency attenuated BBB damage and pyroptosis in SAH mice (A) Bar graphs showed the change in mice performance measured by modified Garcia at 24 h after SAH in WT mice and NLRP3$^{-/-}$ mice (n = 10/group). (B) Bar graphs showed cerebral edema in the left and right hemisphere at 24 h after SAH in WT mice and NLRP3$^{-/-}$ mice (n = 5/group). (C) Bar graphs showed the content of the Evans blue in the left and right hemispheres in WT mice and NLRP3$^{-/-}$ mice (n = 5/group). (D–K) Western blotting images and quantitative data of expression level of ZO-1, occludin, NLRP3, caspase-1, GSDMD-N, IL-1β, and IL-18 in ipsilateral cortex after SAH (n = 5/group). Data was represented as mean ± SD. * mean $P < 0.05$, ** mean $P < 0.01$, *** mean $P < 0.001$ vs sham group.

3.8. CXCR4 inhibition reduced NLRP3-mediated pyroptosis and lipid peroxidation in hemin-treated BV2 in vitro

To further explore the role of CXCR4 in pyroptosis, CXCR4 inhibitor AMD3100 was applicated. When hemin-treated BV2 cells were treated with different concentrations, the results of CCK8 experiments showed that the optimum treatment concentration of AMD3100 is 10uM (Fig. 8A). Immunofluorescence displayed that AMD3100 could significantly reduce BTK phosphorylation in BV2 treated with hemin (Fig. 8B). Western blotting showed that AMD3100 significantly attenuated the expression level of p-BTK, NLRP3, ASC, p-P65, GSDMD-N, IL-1β, IL-18 and NOX2 in BV2 treated with hemin (Fig. 8C–K). Moreover, the results found that AMD3100 can reduce ROS levels in hemin-treated BV2 cells in vitro (Fig. 8L-M). These results further indicated that CXCR4 may regulate NF-κB activation, pyroptosis and oxidative stress by inhibiting BTK phosphorylation in BV2 cells.

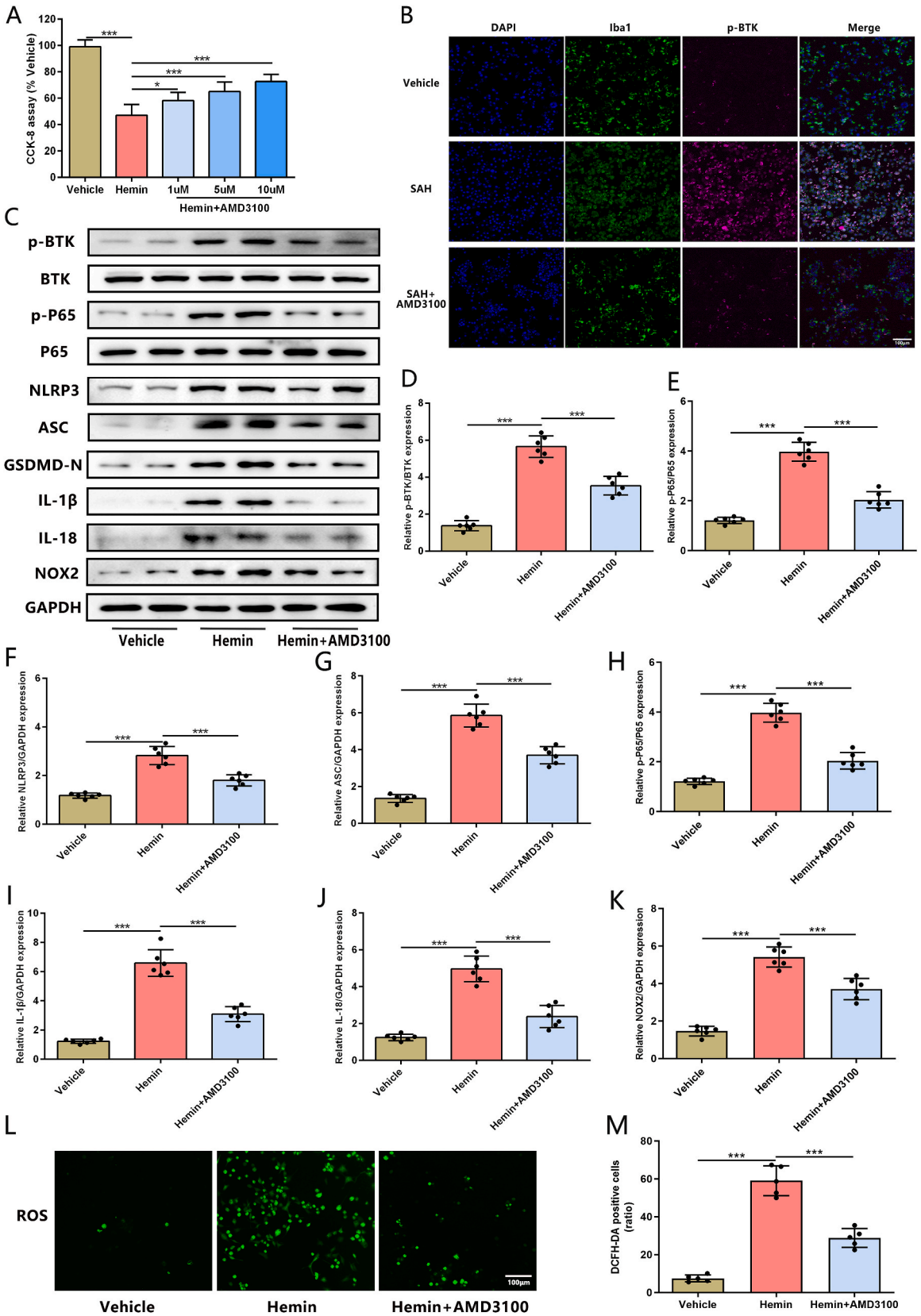

Fig. 8. CXCR4 inhibition reduce NF-κB activation, NLRP3-mediated pyroptosis and oxidative stress in hemin-treated BV2 cells (A) The viability of BV2 cells treated with different concentration of AMD3100 for 24 h was tested by CCK-8 assay in vitro (n = 6/group). (B) Co-staining of Iba (green) and p-BTK (red) was showed in BV2 cells at 24 h after SAH (n = 3/group, original magnification × 200). (C–K) Western blotting images and quantitative data of relative expression level of p-BTK, BTK, p-P65, P65, NLRP3, ASC, GSDMD-N, IL-1β, IL-18 and NOX2 in hemin-treated BV2 cells (n = 6/group). (L) Representative images of ROS expression detected by immunofluorescence in BV2 cells treated with hemin or/and AMD3100 (original magnification × 200). (M) Quantitative analyses of the number of DCFH-DA-positive cells (n = 5/group). Data was represented as mean ± SD. * mean $P < 0.05$, ** mean $P < 0.01$, *** mean $P < 0.001$ vs vehicle group.

3.9. Inhibition of BTK phosphorylation can reverse CXCR4-aggravated BBB damage and inflammation in SAH mouse

To further verify the relationship between BTK and CXCR4, lentivirus OE-CXCR4 was injected by i.c.v to overexpressing CXCR4 *in vivo*. Western blotting showed that overexpression CXCR4 can further aggravate the destruction of ZO-1 and occludin and promote the expression levels of p-BTK, NLRP3, p-P65, GSDMD-N, IL-1β, IL-18 and NOX2 compare with the OE-NC group, while ibrutinib can significantly improve BBB disruption and abolish these increases on p-BTK, p-P65, NLRP3, GSDMD-N, NOX2 and inflammatory cytokines IL-1β and IL-18 (Fig. 9A–K).

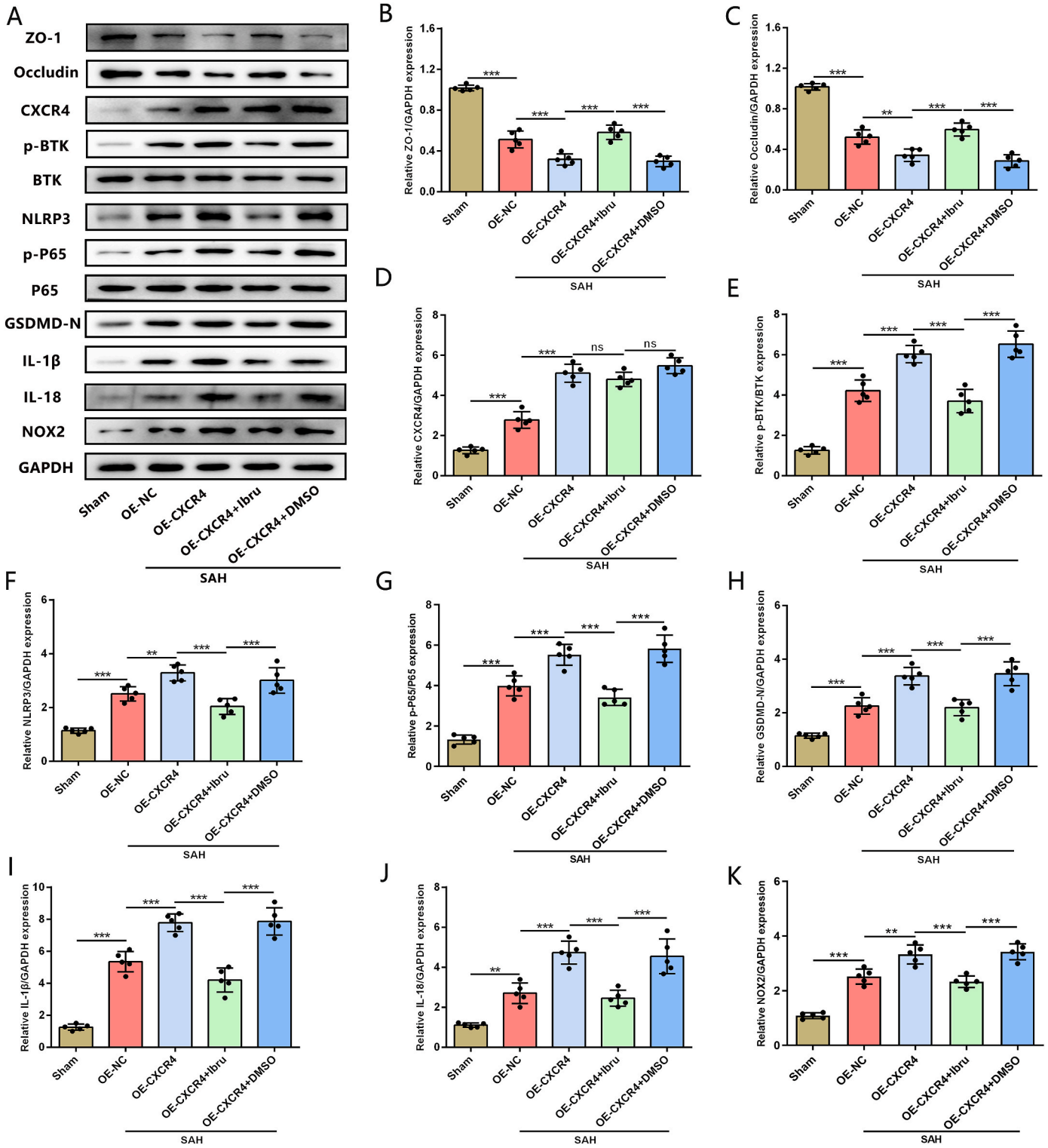

Fig. 9. Ibrutinib can reverse CXCR4-aggravated BBB damage and inflammation in SAH mouse (A–K) Western blotting images and quantitative data of relative protein level of ZO-1, occludin, CXCR4, p-BTK, BTK, p-P65, P65, NLRP3, GSDMD-N, IL-1β, IL-18 and NOX2 (n = 5/group). Data was represented as mean ± SD. * mean $P < 0.05$, ** mean $P < 0.01$, *** mean $P < 0.001$ vs sham group.

3.10. The high correlation between CXCR4 and GSDMD, IL-1β levels and outcomes in human CSF

To clarify the levels of CXCR4, pyroptosis-related protein (GSDMD) and inflammatory factors (IL-1β) in the CSF of patients with SAH, we performed ELISA testing on the CSF of patients with SAH (n = 30) and control (n = 10). The results showed that the levels of CXCR4, GSDMD and IL-1β were significantly increased in the SAH group compared to the control group (Fig. 10A–C). Pearson's correlation coefficient was used to analyze the relationship between CXCR4 levels and GSDMD, IL-1β levels and mRS scores at 6 months after discharge. The results found that CXCR4 was positively correlated with GSDMD (r = 0.2067, $P = 0.0116$) (Fig. 10D), IL-1β (r = 0.3094, $P < 0.001$) (Fig. 10E), and mRS score (r = 0.3135, $P < 0.01$) (Fig. 10F). Moreover, the higher the mRS score was, the higher the level of CXCR4 found in the human CSF (Fig. 10G). Receiver operating characteristic (ROC) curve analysis showed that CXCR4 levels (AUC = 0.85, sensitivity = 90%, specificity = 65%, P = 0.0028) (Fig. 10H) after SAH had a moderate diagnostic value for outcomes at the 6-month follow-up. The cut-off value of CXCR4 was 1903 pg/mL according to the ROC curve.

4. Discussion

This article investigated the role of CXCR4 and BTK phosphorylation in the pathogenesis of pyroptosis after SAH. Our results found that the expression of CXCR4 and p-BTK was up-regulated in microglia after SAH, both *in vivo* and in vitro. Pharmacological blockade of BTK phosphorylation with ibrutinib can significantly attenuate neurological impairments, brain edema, BBB damage, lipid peroxidation and neuronal injury. Ibrutinib treatment reduced microglial pyroptosis and lipid peroxidation by inhibiting NLRP3 inflammasome, NF-κB activation and NOX2 expression. Moreover, the COIP experiment indicated the directly

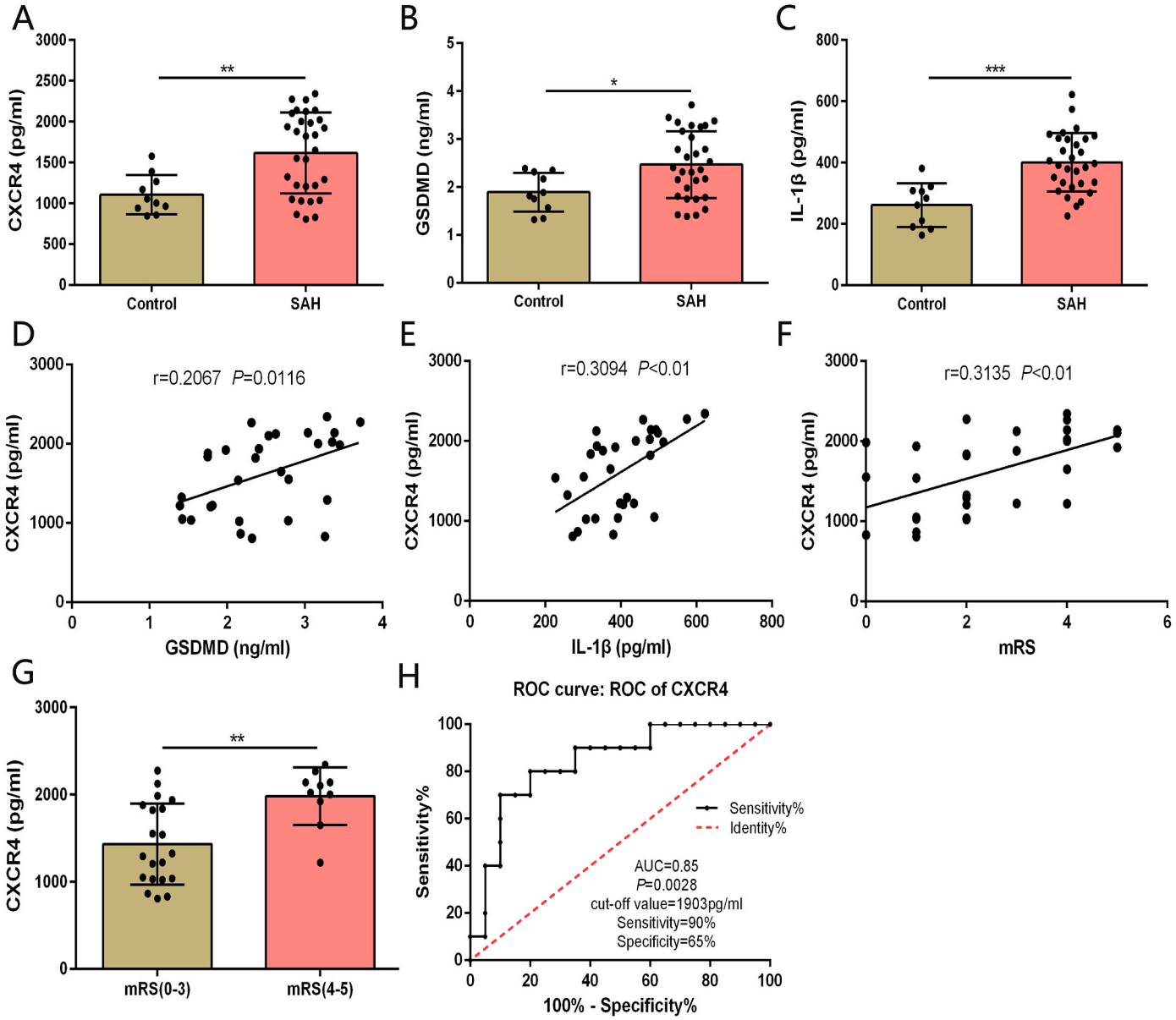

Fig. 10. The expression of CXCR4, GSDMD, and IL-1β in human CSF and the correlation between CXCR4 and GSDMD, IL-1β, and outcome. (A–C) The levels of CXCR4, GSDMD and IL-1β in human CSF were detected by ELISA assay in control (n = 10) and SAH (30) patients. (D–E) The linear-regression analysis showed the relationship between CXCR4 and GSDMD, IL-1β, and mRS scores. (F) ELISA assay for the CXCR4 protein in CSF from SAH patients with different mRS scores (0–3 vs 4–5). (G–H) ROC showed that CXCR4 levels in human CSF after SAH have a moderate diagnostic value for outcome at 6-month follow-up. Data was represented as mean ± SD. *$P < 0.05$, **$P < 0.01$, ***$P < 0.001$ vs control group.

interaction of p-BTK and NLRP3. NLRP3 deficiency exhibited significantly protective role in neurological function and BBB integrity, and inhibited pyroptosis and inflammation after SAH in mice. CXCR4 inhibition can also reduce NF-κB activation, NLRP3-mediated pyroptosis and lipid peroxidation. And ibrutinib can reverse CXCR4-aggravated BBB damage and inflammation. Clinical trial results also indicated that CXCR4 was high correlation with GSDMD, IL-1β levels and unfavorable outcomes in human CSF of SAH patients. These results showed that CXCR4-BTK axis can regulate NLRP3-mediated pyroptosis and lipid peroxidation after subarachnoid hemorrhage via the NF-κB pathway.

The pathophysiology of SAH is complex, and a growing body of evidence implicated that the inflammatory response plays an important role in the pathogenesis of EBI following SAH [42,43]. Activated microglia play vital role in the inflammatory response [44]. Our results suggested that SAH mice developed remarkably inflammatory response with pronounced microglia activation and the release of inflammatory cytokines in ipsilateral cortex. Excessive innate immune responses contribute to BBB damage and neuronal injury after SAH. Therefore, reducing the inflammatory response after SAH is crucial for improving brain injury. Pyroptosis, as a gasdermin-induced programmed cell death, is characterized by the plasma membrane integrity disruption, which contributes to extracellular spilling of inflammatory cytokines [33,45]. The inflammasome is a cytosolic multiprotein complex that mediates inflammation and pyroptosis, which includes NLRP1 and NLRP3 [46,47]. The NLRP3 inflammasome activates caspase-1 to mediate GSDMD-dependent pyroptosis, and facilitate to cleave pro-IL-18 and pro-IL-1β for generating the mature cytokines. A growing number of literatures suggested that inhibition of NLRP3 inflammasome reduces brain injury after SAH [48,49]. GSDMD is the essential pyroptosis mediator, and its N-terminal fragment of GSDMD can oligomerize and bind to the plasma membrane for pyroptotic pore formation [50–53]. Our study found increased levels of GSDMD and IL-1β in CSF of SAH patients. And the expression level of GSDMD-N, IL-1β and IL-18 was also elevated in ipsilateral hemisphere of SAH mice and hemin-treated BV2 cells. Inhibition BTK phosphorylation by ibrutinib significantly suppressed microglial pyroptosis and the secretion of IL-1β and IL-18 both in vivo and in vitro, suggesting that p-BTK regulates microglial pyroptosis following SAH. Moreover, our results demonstrated that p-BTK binds directly to NLRP3 in BV2 cells. Recent research also suggested that BTK can directly regulate NLRP3 phosphorylation, thereby affecting the formation of NLRP3 inflammasome [18,54]. NLRP3 deficiency could attenuate neurological impairment, cerebral edema, BBB disruption and inflammatory response in SAH mice. The results suggested that p-BTK can directly bind NLRP3 and regulated NLRP3-mediated pyroptosis after SAH.

Increasing evidence suggested that BTK presented in myeloid cells, including microglia, is a key regulator of the innate immune system [14]. BTK inhibition significantly inhibits the degradation of IκBα, decreases the nuclear accumulation of p–NF–κB, and downstream the expression of inflammation cytokines [55–57]. NF-κB can regulate the expression of NLRP3 protein and the mRNA level of IL-1β and IL-18 [58]. Attenuation of the NF-κB-activated NOD-like receptor signaling pathway inhibited the cytoplasmic secretion of IL-18 and IL-1β and decreased the expression of pyroptosis markers (NLRP3, GSDMD, and caspase-1) [59]. In addition, microglia M1/M2 polarization was activated by the TLR4-mediated NF-κB signaling pathway [60]. Inhibiting the nuclear entry of NF-κB can regulate the microglia polarization equilibrium, and promote M2 polarization after treatment with LPS [61]. BTK can trigger the expression and release of pro-inflammatory cytokines in macrophages and neutrophils. BTK inhibition attenuates the inflammatory response in a variety of diseases, including arthritis, pneumonia and sepsis [13,62,63]. Our results also showed that p-BTK was significantly upregulated in microglia after SAH. Inhibition of BTK phosphorylation with ibrutinib reduced the release of inflammatory cytokines, prevented neurological impairment, damage of tight junction proteins, lipid peroxidation and neuronal injury, and significantly improved 7-day survival after SAH. BTK phosphorylation inhibition can significantly attenuate the level of p–NF–κB and promote the transition of M1-polarized microglia to M2 in vitro after hemin treatment. These results implicated that BTK phosphorylation can promote inflammatory response after SAH by regulating the NF-κB pathway. In addition, our results showed that BTK phosphorylation inhibition reduced the level of lipid peroxidation after SAH in vitro *and vivo*. To further explore the role of BTK in regulating lipid peroxidation, we found that BTK phosphorylation inhibition reduced NOX2 expression. NOX2, an NADPH oxidase, is widely expressed in the brain and plays an important role in ROS generation [64,65]. It has been reported that NF-κB activation can promote lipid peroxidation by promoting NOX2 expression in high-fat-diet-fed mice [66]. Therefore, BTK phosphorylation may regulate ROS generation by promoting NOX2 expression through NF-κB activation. Other literatures have reported that NOX2-induced ROS also regulates inflammation by activating NF-KB [67,68]. Therefore, BTK may be an important target for regulating inflammation and lipid peroxidation.

CXCR4, as one of the G protein-coupled receptor, is critical for homeostasis of the adaptive and innate immune system in CNS diseases, such as intracerebral hemorrhage [24], ischemic stroke [69], Alzheimer's disease [70], Parkinson's disease [71], and traumatic brain injury [26]. However, the role of CXCR4 in stroke is controversial. Some studies have found that blocking CXCR4 can reduce macrophage infiltration, microglia activation and inflammatory response in acute cerebral ischemia, while CXCR4 knockout reduces inflammatory cell clearance and vascular growth, which is not conducive to long-term prognosis in mice [72,73]. Previous studies have also showed that CXCR4 can participate in the process of pyroptosis [74]. Nevertheless, how CXCR4 affects pyroptosis in acute brain injury is unclear. In the present study, our results found that the expression of CXCR4 increased significantly at 24 h after SAH in vivo and in vitro. AMD3100 can also inhibit NLRP3-mediated pyroptosis, NF-κB activation and NOX2 expression in vitro, and ibrutinib can abolish CXCR4-aggravated pyroptosis and lipid peroxidation in EBI after SAH. These results indicated that CXCR4 can mediate NLRP3-related pyroptosis and NF-κB activation by regulating BTK phosphorylation. In addition, the levels of CXCR4, GSDMD and IL-1β in human CSF was tested by ELISA kits. The results indicated that the level of CXCR4 in CSF of SAH patients is significantly increased, and it is positively correlated with GSDMD and IL-1β levels, and have a moderate diagnostic value for outcome at 6-month follow-up. Above results revealed that CXCR4 plays an important role in the inflammatory process, and inhibition of CXCR4-BTK axis can effectively reduce neuroinflammation, pyroptosis and lipid peroxidation in EBI after SAH. Interestingly, long-term administration of AMD3100 has been shown to reduce immune cell entry and immune cell activation after cerebral ischemia, but also reduce microvessel formation [72]. Therefore, long-term use of AMD3100 in the treatment of brain injury requires caution.

Nevertheless, there are some limitations in this study. First, we focused on the role of CXCR4-BTK axis in microglia after SAH. However, with the infiltration and action of various immune cells after SAH, the role of CXCR4-p-BTK axis in other immune cells needs to be further investigated. Second, to further clarify the role of NLRP3 in pyroptosis after SAH, NLRP3 knockout mice were used to verify its effects on neurological function and pyroptosis pathway. Microglia-specific NLRP3 knockout mice may be a better choice. Nevertheless, due to the limitation of experimental conditions, we will explore this in future studies.

In this study, we found the effect of CXCR4 and P-BTK on NLRP3-mediated pyroptosis in vivo and in vitro, and the potential diagnostic role of CXCR4 in CSF of SAH patients. Inhibition of CXCR4-BTK axis can significantly attenuate neuroinflammation and lipid peroxidation by regulating NLRP3-mediated pyroptosis and NF-κB activation in EBI after SAH. Therefore, CXCR4-BTK might provide a promising treatment strategy for neuroinflammation and lipid peroxidation in SAH patients.

Author's contribution

Chengli Liu, Kun Yao and Qi Tian designed and completed the study, conducted data analysis, and prepared the manuscript. Yujia Guo, Guijun Wang, Peibang He, Jianfeng Wang and Jian Wang built SAH models in mice and completed some experiments. Zhan Zhang and Mingchang Li reviewed and revised the manuscript.

Declaration of competing interest

The authors declare that they have no conflict of interest.

Data availability

Data will be made available on request.

Acknowledgements

We thank Professor Xiaoxing Xiong of our department for the gift of NLRP3$^{-/-}$ mice. This article was supported by grants from the National Natural Science Foundation of China (No. 81971870 and No. 82172173).

Appendix A. Supplementary data

Supplementary data to this article can be found online at https://doi.org/10.1016/j.redox.2023.102960.

References

[1] N. Etminan, H.S. Chang, K. Hackenberg, N.K. de Rooij, M. Vergouwen, G. Rinkel, A. Algra, Worldwide incidence of aneurysmal subarachnoid hemorrhage according to region, time period, blood pressure, and smoking prevalence in the population: a systematic review and meta-analysis, JAMA Neurol. 76 (2019) 588–597.

[2] R. Gu, L. Wang, H. Zhou, X. Wang, C. Lenahan, H. Qu, Y. Liu, S. Li, C. Wei, L. Han, X. Hu, G. Zuo, Rh-CXCL-12 attenuates neuronal pyroptosis after subarachnoid hemorrhage in rats via regulating the CXCR4/NLRP1 pathway, Oxid. Med. Cell. Longev. (2021), 6966394, 2021.

[3] K. Kumagai, A. Tomiyama, S. Takeuchi, N. Otani, M. Fujita, K. Fujii, K. Wada, K. Mori, New endovascular perforation subarachnoid hemorrhage model for investigating the mechanisms of delayed brain injury, J. Neurosurg. 1–11 (2019).

[4] C. Zhang, M. Jiang, W.Q. Wang, S.J. Zhao, Y.X. Yin, Q.J. Mi, M.F. Yang, Y.Q. Song, B.L. Sun, Z.Y. Zhang, Selective mGluR1 negative allosteric modulator reduces blood-brain barrier permeability and cerebral edema after experimental subarachnoid hemorrhage, Transl Stroke Res 11 (2020) 799–811.

[5] Z.V. Zheng, H. Lyu, S. Lam, P.K. Lam, W.S. Poon, G. Wong, The dynamics of microglial polarization reveal the resident neuroinflammatory responses after subarachnoid hemorrhage, Transl Stroke Res 11 (2020) 433–449.

[6] B.P. Lucke-Wold, A.F. Logsdon, B. Manoranjan, R.C. Turner, E. McConnell, G. E. Vates, J.D. Huber, C.L. Rosen, J.M. Simard, Aneurysmal subarachnoid hemorrhage and neuroinflammation: a comprehensive review, Int. J. Mol. Sci. 17 (2016) 497.

[7] B. Yuan, X.M. Zhou, Z.Q. You, W.D. Xu, J.M. Fan, S.J. Chen, Y.L. Han, Q. Wu, X. Zhang, Inhibition of AIM2 inflammasome activation alleviates GSDMD-induced pyroptosis in early brain injury after subarachnoid haemorrhage, Cell Death Dis. 11 (2020) 76.

[8] J.P. de Rivero Vaccari, W.D. Dietrich, R.W. Keane, Activation and regulation of cellular inflammasomes: gaps in our knowledge for central nervous system injury, J. Cerebr. Blood Flow Metabol. 34 (2014) 369–375.

[9] K. Zhao, R. An, Q. Xiang, G. Li, K. Wang, Y. Song, Z. Liao, S. Li, W. Hua, X. Feng, X. Wu, Y. Zhang, A. Das, C. Yang, Acid-sensing ion channels regulate nucleus pulposus cell inflammation and pyroptosis via the NLRP3 inflammasome in intervertebral disc degeneration, Cell Prolif. 54 (2021), e12941.

[10] H. Kambara, F. Liu, X. Zhang, P. Liu, B. Bajrami, Y. Teng, L. Zhao, S. Zhou, H. Yu, W. Zhou, L.E. Silberstein, T. Cheng, M. Han, Y. Xu, H.R. Luo, Gasdermin D exerts anti-inflammatory effects by promoting neutrophil death, Cell Rep. 22 (2018) 2924–2936.

[11] Y. Fang, X. Wang, J. Lu, H. Shi, L. Huang, A. Shao, A. Zhang, Y. Liu, R. Ren, C. Lenahan, J. Tang, J. Zhang, J.H. Zhang, S. Chen, Inhibition of caspase-1-mediated inflammasome activation reduced blood coagulation in cerebrospinal fluid after subarachnoid haemorrhage, EBioMedicine 76 (2022), 103843.

[12] P. Xu, C. Tao, Y. Zhu, G. Wang, L. Kong, W. Li, R. Li, J. Li, C. Zhang, L. Wang, X. Liu, W. Sun, W. Hu, TAK1 mediates neuronal pyroptosis in early brain injury after subarachnoid hemorrhage, J. Neuroinflammation 18 (2021) 188.

[13] H.Y. Nam, J.H. Nam, G. Yoon, J.Y. Lee, Y. Nam, H.J. Kang, H.J. Cho, J. Kim, H. S. Hoe, Ibrutinib suppresses LPS-induced neuroinflammatory responses in BV2 microglial cells and wild-type mice, J. Neuroinflammation 15 (2018) 271.

[14] M. Ito, T. Shichita, M. Okada, R. Komine, Y. Noguchi, A. Yoshimura, R. Morita, Bruton's tyrosine kinase is essential for NLRP3 inflammasome activation and contributes to ischaemic brain injury, Nat. Commun. 6 (2015) 7360.

[15] A. Bercusson, T. Colley, A. Shah, A. Warris, D. Armstrong-James, Ibrutinib blocks Btk-dependent NF-κB and NFAT responses in human macrophages during Aspergillus fumigatus phagocytosis, Blood 132 (2018) 1985–1988.

[16] J. Ní Gabhann, E. Hams, S. Smith, C. Wynne, J.C. Byrne, K. Brennan, S. Spence, A. Kissenpfennig, J.A. Johnston, P.G. Fallon, C.A. Jefferies, Btk regulates macrophage polarization in response to lipopolysaccharide, PLoS One 9 (2014), e85834.

[17] M. Pontoriero, G. Fiume, E. Vecchio, A. de Laurentiis, F. Albano, E. Iaccino, S. Mimmi, A. Pisano, V. Agosti, E. Giovannone, A. Altobelli, C. Caiazza, M. Mallardo, G. Scala, I. Quinto, Activation of NF-κB in B cell receptor signaling through Bruton's tyrosine kinase-dependent phosphorylation of IκB-α, J. Mol. Med. (Berl.) 97 (2019) 675–690.

[18] Z.A. Bittner, X. Liu, M. Mateo Tortola, A. Tapia-Abellán, S. Shankar, L. Andreeva, M. Mangan, M. Spalinger, H. Kalbacher, P. Düwell, M. Lovotti, K. Bosch, S. Dickhöfer, A. Marcu, S. Stevanović, F. Herster, Y. Cardona Gloria, T.H. Chang, F. Bork, C.L. Greve, M.W. Löffler, O.O. Wolz, N.A. Schilling, J.B. Kümmerle-Deschner, S. Wagner, A. Delor, B. Grimbacher, O. Hantschel, M. Scharl, H. Wu, E. Latz, A. Weber, BTK operates a phospho-tyrosine switch to regulate NLRP3 inflammasome activity, J. Exp. Med. 218 (2021).

[19] Z. Liu, L. Gan, Y. Xu, D. Luo, Q. Ren, S. Wu, C. Sun, Melatonin alleviates inflammasome-induced pyroptosis through inhibiting NF-κB/GSDMD signal in mice adipose tissue, J. Pineal Res. 63 (2017).

[20] L. Peng, L. Wen, Q.F. Shi, F. Gao, B. Huang, J. Meng, C.P. Hu, C.M. Wang, Scutellarin ameliorates pulmonary fibrosis through inhibiting NF-κB/NLRP3-mediated epithelial-mesenchymal transition and inflammation, Cell Death Dis. 11 (2020) 978.

[21] R. Yu, S. Jiang, Y. Tao, P. Li, J. Yin, Q. Zhou, Inhibition of HMGB1 improves necrotizing enterocolitis by inhibiting NLRP3 via TLR4 and NF-κB signaling pathways, J. Cell. Physiol. 234 (2019) 13431–13438.

[22] A.P. de Porto, Z. Liu, R. de Beer, S. Florquin, O.J. de Boer, R.W. Hendriks, T. van der Poll, A.F. de Vos, Btk inhibitor ibrutinib reduces inflammatory myeloid cell responses in the lung during murine pneumococcal pneumonia, Mol. Med. 25 (3) (2019).

[23] N.O. Al-Harbi, A. Nadeem, S.F. Ahmad, S.A. Bakheet, A.M. El-Sherbeeny, K. E. Ibrahim, K.S. Alzahrani, M.M. Al-Harbi, H.M. Mahmood, F. Alqahtani, S. M. Attia, M.R. Alotaibi, Therapeutic treatment with Ibrutinib attenuates imiquimod-induced psoriasis-like inflammation in mice through downregulation of oxidative and inflammatory mediators in neutrophils and dendritic cells, Eur. J. Pharmacol. 877 (2020), 173088.

[24] S.J. Yu, K.J. Wu, Y.S. Wang, J.S. Song, C.H. Wu, J.J. Jan, et al., Protective effect of CXCR4 antagonist CX807 in a rat model of hemorrhagic stroke, Int. J. Mol. Sci. 21 (19) (2020), https://doi.org/10.3390/ijms21197085.

[25] H.L. Walter, G. van der Maten, A.R. Antunes, T. Wieloch, K. Ruscher, Treatment with AMD3100 attenuates the microglial response and improves outcome after experimental stroke, J. Neuroinflammation 12 (2015) 24, https://doi.org/10.1186/s12974-014-0232-1.

[26] S. Liraz-Zaltsman, Y. Friedman-Levi, D. Shabashov-Stone, G. Gincberg, D. Atrakcy-Baranes, M.T. Joy, et al., Chemokine receptors CC chemokine receptor 5 and C-X-C motif chemokine receptor 4 are new therapeutic targets for brain recovery after traumatic brain injury, J. Neurotrauma 38 (14) (2021) 2003–2017, https://doi.org/10.1089/neu.2020.7015.

[27] K.J. Wu, S.J. Yu, K.S. Shia, C.H. Wu, J.S. Song, H.H. Kuan, et al., A novel CXCR4 antagonist CX549 induces neuroprotection in stroke brain, Cell Transplant. 26 (4) (2017) 571–583, https://doi.org/10.3727/096368916X693563.

[28] S.S. Chen, B.Y. Chang, S. Chang, T. Tong, S. Ham, B. Sherry, et al., BTK inhibition results in impaired CXCR4 chemokine receptor surface expression, signaling and function in chronic lymphocytic leukemia, Leukemia 30 (4) (2016) 833–843, https://doi.org/10.1038/leu.2015.316.

[29] J. Leberzammer, S.M. Agten, X. Blanchet, R. Duan, H. Ippel, R. Megens, et al., Targeting platelet-derived CXCL12 impedes arterial thrombosis, Blood 139 (17) (2022) 2691–2705, https://doi.org/10.1182/blood.2020010140.

[30] Q. Tian, Y. Guo, S. Feng, C. Liu, P. He, J. Wang, et al., Inhibition of CCR2 attenuates neuroinflammation and neuronal apoptosis after subarachnoid hemorrhage through the PI3K/Akt pathway, J. Neuroinflammation 19 (1) (2022) 312, https://doi.org/10.1186/s12974-022-02676-8.

[31] J. Chen, C. Zhang, T. Yan, L. Yang, Y. Wang, Z. Shi, M. Li, Q. Chen, Atorvastatin ameliorates early brain injury after subarachnoid hemorrhage via inhibition of pyroptosis and neuroinflammation, J. Cell. Physiol. 236 (2021) 6920–6931.

[32] L. Zhou, F. Li, H.B. Xu, C.X. Luo, H.Y. Wu, M.M. Zhu, et al., Treatment of cerebral ischemia by disrupting ischemia-induced interaction of nNOS with PSD-95, Nat. Med. 16 (12) (2010) 1439–1443, https://doi.org/10.1038/nm.2245.

[33] P. Xu, Y. Hong, Y. Xie, K. Yuan, J. Li, R. Sun, X. Zhang, X. Shi, R. Li, J. Wu, X. Liu, W. Hu, W. Sun, TREM-1 exacerbates neuroinflammatory injury via NLRP3 inflammasome-mediated pyroptosis in experimental subarachnoid hemorrhage, Transl Stroke Res 12 (2021) 643–659.

[34] S. Li, X. Hua, M. Zheng, J. Wu, Z. Ma, X. Xing, J. Ma, J. Zhang, C. Shan, J. Xu, PLXNA2 knockdown promotes M2 microglia polarization through mTOR/STAT3 signaling to improve functional recovery in rats after cerebral ischemia/reperfusion injury, Exp. Neurol. 346 (2021), 113854.

[35] C. Liu, S. Sun, J. Xie, H. Li, T. Li, Q. Wu, Y. Zhang, X. Bai, J. Wang, X. Wang, Z. Li, W. Wang, GLP-1R agonist exendin-4 protects against hemorrhagic transformation induced by rtPA after ischemic stroke via the Wnt/β-catenin signaling pathway, Mol. Neurobiol. 59 (2022) 3649–3664.

[36] A. Yasmin, A. Pitkänen, P. Andrade, T. Paananen, O. Gröhn, R. Immonen, Post-injury ventricular enlargement associates with iron in choroid plexus but not with seizure susceptibility nor lesion atrophy-6-month MRI follow-up after experimental traumatic brain injury, Brain Struct. Funct. 227 (2022) 145–158.
[37] P. Gong, Z. Zhang, C. Zou, Q. Tian, X. Chen, M. Hong, et al., Hippo/YAP signaling pathway mitigates blood-brain barrier disruption after cerebral ischemia/reperfusion injury, Behav. Brain Res. 356 (2019) 8–17, https://doi.org/10.1016/j.bbr.2018.08.003.
[38] S. Li, Z. Tian, X. Xian, et al., Catalpol rescues cognitive deficits by attenuating amyloid β plaques and neuroinflammation, Biomed. Pharmacother. (2023) 165 115026, https://doi.org/10.1016/j.biopha.2023.115026.
[39] J. Kim, H.J. Lee, J.H. Park, et al., Nilotinib modulates LPS-induced cognitive impairment and neuroinflammatory responses by regulating P38/STAT3 signaling, J. Neuroinflammation 19 (2022) 187, https://doi.org/10.1186/s12974-022-02549-0.
[40] C. Liu, P. He, Y. Guo, et al., Taurine attenuates neuronal ferroptosis by regulating GABA(B)/AKT/GSK3β/β-catenin pathway after subarachnoid hemorrhage, Free Radic. Biol. Med. 193 (2022) 795–807, https://doi.org/10.1016/j.freeradbiomed.2022.11.003.
[41] H. Song, B. Liu, W. Huai, Z. Yu, W. Wang, J. Zhao, L. Han, G. Jiang, L. Zhang, C. Gao, W. Zhao, The E3 ubiquitin ligase TRIM31 attenuates NLRP3 inflammasome activation by promoting proteasomal degradation of NLRP3, Nat. Commun. 7 (2016), 13727.
[42] A.P. Coulibaly, J.J. Provencio, Aneurysmal subarachnoid hemorrhage: an overview of inflammation-induced cellular changes, Neurotherapeutics 17 (2020) 436–445.
[43] U.C. Schneider, R. Xu, P. Vajkoczy, Inflammatory events following subarachnoid hemorrhage (SAH), Curr. Neuropharmacol. 16 (2018) 1385–1395.
[44] J. Chen, Z.V. Zheng, G. Lu, W.Y. Chan, Y. Zhang, G. Wong, Microglia activation, classification and microglia-mediated neuroinflammatory modulators in subarachnoid hemorrhage, Neural Regen Res 17 (2022) 1404–1411.
[45] J. Shi, W. Gao, F. Shao, Pyroptosis: gasdermin-mediated programmed necrotic cell death, Trends Biochem. Sci. 42 (2017) 245–254.
[46] Y. Huang, W. Xu, R. Zhou, NLRP3 inflammasome activation and cell death, Cell. Mol. Immunol. 18 (2021) 2114–2127.
[47] Y. Xue, D. Enosi Tuipulotu, W.H. Tan, C. Kay, S.M. Man, Emerging activators and regulators of inflammasomes and pyroptosis, Trends Immunol. 40 (2019) 1035–1052.
[48] W.S. Dodd, I. Noda, M. Martinez, K. Hosaka, B.L. Hoh, NLRP3 inhibition attenuates early brain injury and delayed cerebral vasospasm after subarachnoid hemorrhage, J. Neuroinflammation 18 (2021) 163.
[49] J.R. Li, H.Z. Xu, S. Nie, Y.C. Peng, L.F. Fan, Z.J. Wang, C. Wu, F. Yan, J.Y. Chen, C. Gu, C. Wang, J.S. Chen, L. Wang, G. Chen, Fluoxetine-enhanced autophagy ameliorates early brain injury via inhibition of NLRP3 inflammasome activation following subrachnoid hemorrhage in rats, J. Neuroinflammation 14 (2017) 186.
[50] J. Ding, K. Wang, W. Liu, Y. She, Q. Sun, J. Shi, H. Sun, D.C. Wang, F. Shao, Pore-forming activity and structural autoinhibition of the gasdermin family, Nature 535 (2016) 111–116.
[51] W.T. He, H. Wan, L. Hu, P. Chen, X. Wang, Z. Huang, Z.H. Yang, C.Q. Zhong, J. Han, Gasdermin D is an executor of pyroptosis and required for interleukin-1β secretion, Cell Res. 25 (2015) 1285–1298.
[52] L. Sborgi, S. Rühl, E. Mulvihill, J. Pipercevic, R. Heilig, H. Stahlberg, C.J. Farady, D.J. Müller, P. Broz, S. Hiller, GSDMD membrane pore formation constitutes the mechanism of pyroptotic cell death, EMBO J. 35 (2016) 1766–1778.
[53] K. Wang, Q. Sun, X. Zhong, M. Zeng, H. Zeng, X. Shi, Z. Li, Y. Wang, Q. Zhao, F. Shao, J. Ding, Structural mechanism for GSDMD targeting by autoprocessed caspases in pyroptosis, Cell 180 (2020) 941–955.e20.
[54] L. Mao, A. Kitani, E. Hiejima, K. Montgomery-Recht, W. Zhou, I. Fuss, A. Wiestner, W. Strober, Bruton tyrosine kinase deficiency augments NLRP3 inflammasome activation and causes IL-1β-mediated colitis, J. Clin. Invest. 130 (2020) 1793–1807.
[55] Z. Fan, Y. Wang, X. Xu, Y. Wu, Inhibitor of Bruton's tyrosine kinases, PCI-32765, decreases pro-inflammatory mediators' production in high glucose-induced macrophages, Int. Immunopharm. 58 (2018) 145–153.
[56] S.E. Herman, R.Z. Mustafa, J.A. Gyamfi, S. Pittaluga, S. Chang, B. Chang, M. Farooqui, A. Wiestner, Ibrutinib inhibits BCR and NF-κB signaling and reduces tumor proliferation in tissue-resident cells of patients with CLL, Blood 123 (2014) 3286–3295.
[57] C. Yue, M. Niu, Q.Q. Shan, T. Zhou, Y. Tu, P. Xie, L. Hua, R. Yu, X. Liu, High expression of Bruton's tyrosine kinase (BTK) is required for EGFR-induced NF-κB activation and predicts poor prognosis in human glioma, J. Exp. Clin. Cancer Res. 36 (2017) 132.
[58] D. Peng, J. Li, Y. Deng, X. Zhu, L. Zhao, Y. Zhang, Z. Li, S. Ou, S. Li, Y. Jiang, Sodium para-aminosalicylic acid inhibits manganese-induced NLRP3 inflammasome-dependent pyroptosis by inhibiting NF-κB pathway activation and oxidative stress, J. Neuroinflammation 17 (2020) 343.
[59] H. Tao, W. Li, W. Zhang, C. Yang, C. Zhang, X. Liang, J. Yin, J. Bai, G. Ge, H. Zhang, X. Yang, H. Li, Y. Xu, Y. Hao, Y. Liu, D. Geng, Urolithin A suppresses RANKL-induced osteoclastogenesis and postmenopausal osteoporosis by, suppresses inflammation and downstream NF-κB activated pyroptosis pathways, Pharmacol. Res. 174 (2021), 105967.
[60] M. Huang, Y. Li, K. Wu, W. Yan, T. Tian, Y. Wang, H. Yang, Paraquat modulates microglia M1/M2 polarization via activation of TLR4-mediated NF-κB signaling pathway, Chem. Biol. Interact. 310 (2019), 108743.
[61] J.Q. Liu, M. Zhao, Z. Zhang, L.Y. Cui, X. Zhou, W. Zhang, S.F. Chu, D.Y. Zhang, N. H. Chen, Rg1 improves LPS-induced Parkinsonian symptoms in mice via inhibition of NF-κB signaling and modulation of M1/M2 polarization, Acta Pharmacol. Sin. 41 (2020) 523–534.
[62] J. Qiu, Y. Fu, Z. Chen, L. Zhang, L. Li, D. Liang, F. Wei, Z. Wen, Y. Wang, S. Liang, BTK promotes atherosclerosis by regulating oxidative stress, mitochondrial injury, and ER stress of macrophages, Oxid. Med. Cell. Longev. (2021), 9972413, 2021.
[63] C.G. Yu, V. Bondada, H. Iqbal, K.L. Moore, J.C. Gensel, S. Bondada, J.W. Geddes, Inhibition of Bruton tyrosine kinase reduces neuroimmune cascade and promotes recovery after spinal cord injury, Int. J. Mol. Sci. 23 (2021).
[64] W. Tao, L. Yu, S. Shu, et al., miR-204-3p/Nox4 mediates memory deficits in a mouse model of Alzheimer's disease, Mol. Ther. 29 (2021) 396–408, https://doi.org/10.1016/j.ymthe.2020.09.006.
[65] Y. Yingze, J. Zhihong, J. Tong, et al., NOX2-mediated reactive oxygen species are double-edged swords in focal cerebral ischemia in mice, J. Neuroinflammation 19 (2022) 184, https://doi.org/10.1186/s12974-022-02551-6.
[66] A.M. Cheriyan, A.C. Ume, C.E. Francis, et al., Calcineurin A-α suppression drives nuclear factor-κB-mediated NADPH oxidase-2 upregulation, Am. J. Physiol. Ren. Physiol. (2021), https://doi.org/10.1152/ajprenal.00254.2020, 320 F789-789F798.
[67] J.M. Yao, H.Z. Ying, H.H. Zhang, et al., Exosomal RBP4 potentiated hepatic lipid accumulation and inflammation in high-fat-diet-fed mice by promoting M1 polarization of Kupffer cells, Free Radic. Biol. Med. (2023), https://doi.org/10.1016/j.freeradbiomed.2022.12.085, 195 58-73.
[68] N.Y. Kim, S. Kim, H.M. Park, et al., Cinnamomum verum extract inhibits NOX2/ROS and PKCδ/JNK/AP-1/NF-κB pathway-mediated inflammatory response in PMA-stimulated THP-1 monocytes, Phytomedicine (2023) 112 154685, https://doi.org/10.1016/j.phymed.2023.154685.
[69] M. Huang, Y. Wan, L. Mao, Q.W. He, Y.P. Xia, M. Li, et al., Inhibiting the migration of M1 microglia at hyperacute period could improve outcome of tMCAO rats, CNS Neurosci. Ther. 23 (3) (2017) 222–232, https://doi.org/10.1111/cns.12665.
[70] J. Ma, Z. Wang, S. Chen, W. Sun, Q. Gu, D. Li, et al., EphA1 activation induces neuropathological changes in a mouse model of Parkinson's disease through the CXCL12/CXCR4 signaling pathway, Mol. Neurobiol. 58 (3) (2021) 913–925, https://doi.org/10.1007/s12035-020-02122-x.
[71] J. Ma, L. Dong, Q. Chang, S. Chen, J. Zheng, D. Li, et al., CXCR4 knockout induces neuropathological changes in the MPTP-lesioned model of Parkinson's disease, Biochim. Biophys. Acta, Mol. Basis Dis. 1869 (2) (2023), 166597, https://doi.org/10.1016/j.bbadis.2022.166597.
[72] Y. Werner, E. Mass, P. Ashok Kumar, et al., Cxcr4 distinguishes HSC-derived monocytes from microglia and reveals monocyte immune responses to experimental stroke, Nat. Neurosci. 23 (2020) 351–362, https://doi.org/10.1038/s41593-020-0585-y.
[73] M. Gao, Q. Dong, H. Yao, Y. Zhang, Y. Yang, Y. Dang, et al., Induced neural stem cells modulate microglia activation states via CXCL12/CXCR4 signaling, Brain Behav. Immun. 59 (2017) 288–299, https://doi.org/10.1016/j.bbi.2016.09.020.
[74] E. Rioja-Blanco, I. Arroyo-Solera, P. Álamo, I. Casanova, A. Gallardo, U. Unzueta, et al., CXCR4-targeted nanotoxins induce GSDME-dependent pyroptosis in head and neck squamous cell carcinoma, J. Exp. Clin. Cancer Res. 41 (1) (2022) 49, https://doi.org/10.1186/s13046-022-02267-8.